



NTNU – Trondheim
Norwegian University of
Science and Technology

Experimental study of density waves oscillations

Luis Ugueto

Master's Thesis

Submission date: June 2013

Supervisor: Carlos Alberto Dorao, EPT

Norwegian University of Science and Technology
Department of Energy and Process Engineering



NTNU – Trondheim
Norwegian University of
Science and Technology

Experimental Study of Density Wave Oscillations

Luis Ugueto

Master's Thesis

Submission date: June 2013

Supervisor: Carlos Dorao

Norwegian University of Science and Technology
Department of Energy and Process Engineering

EPT-M-2013-129

MASTER THESIS

for

Stud.techn Luis Ugueto
Spring 2013

Experimental study of density waves oscillations

*Eksperimentell studie av tetthet bølger svingninger***Background and objective**

Density Wave Oscillation (DWO) are one of the main types of two-phase flow dynamic oscillations frequently encountered in industrial thermal-hydraulic systems. The self-sustained DWO may cause many undesired problems such as mechanical and thermal fatigue of components by mechanical vibration and thermal waves. To avoid or control density-wave oscillations is critical for two-phase systems, but unfortunately, there is not a perfect criterion to predict the stability of two-phase systems or correlations to calculate amplitude and period of DWO.

In this work an experimental work will be performed for studying the stability of the two phase flow system. The main purpose will be to identify how the operational parameters affect the characteristic of the DWO.

The following tasks are to be considered:

- 1 Literature review on DWO
- 2 Preparation of the experiment, data acquisition, error analysis, and data processing

-- " --

Within 14 days of receiving the written text on the master thesis, the candidate shall submit a research plan for his project to the department.

When the thesis is evaluated, emphasis is put on processing of the results, and that they are presented in tabular and/or graphic form in a clear manner, and that they are analyzed carefully.

The thesis should be formulated as a research report with summary both in English and Norwegian, conclusion, literature references, table of contents etc. During the preparation of the text, the candidate should make an effort to produce a well-structured and easily readable report. In order to ease the evaluation of the thesis, it is important that the cross-references are correct. In the making of the report, strong emphasis should be placed on both a thorough discussion of the results and an orderly presentation.

The candidate is requested to initiate and keep close contact with his/her academic supervisor(s) throughout the working period. The candidate must follow the rules and regulations of NTNU as well as passive directions given by the Department of Energy and Process Engineering.

Risk assessment of the candidate's work shall be carried out according to the department's procedures. The risk assessment must be documented and included as part of the final report. Events related to the candidate's work adversely affecting the health, safety or security, must be documented and included as part of the final report. If the documentation on risk assessment represents a large number of pages, the full version is to be submitted electronically to the supervisor and an excerpt is included in the report.

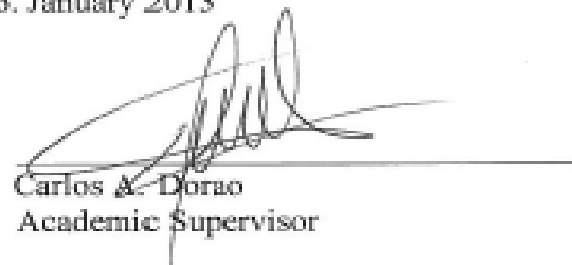
Pursuant to "Regulations concerning the supplementary provisions to the technology study program/Master of Science" at NTNU §20, the Department reserves the permission to utilize all the results and data for teaching and research purposes as well as in future publications.

The final report is to be submitted digitally in DAIM. An executive summary of the thesis including title, student's name, supervisor's name, year, department name, and NTNU's logo and name, shall be submitted to the department as a separate pdf file. Based on an agreement with the supervisor, the final report and other material and documents may be given to the supervisor in digital format.

- Work to be done in lab (Water power lab, Fluids engineering lab, Thermal engineering lab)
 Field work

Department of Energy and Process Engineering, 16. January 2013


Olav Bolland
Department Head


Carlos A. Dorao
Academic Supervisor

Research Advisors: Ezequiel Manavela Chiapero
Han Deng

To my parents, Luis and Marbely

ABSTRACT

Nowadays, systems based on convective boiling flows are found in a wide variety of industrial applications, such as boiling water reactors, boilers, thermosiphons, heat exchangers, condenser, chemical reactors and some other chemical process units. Such systems take advantage of the high heat transfer rates that a boiling fluid can reach at moderate temperature differences. However, those systems are unfortunately susceptible to thermally induced two-phase flow instabilities, such as Density Wave Oscillations. Thereby, the aim of present research is to perform an experimental investigation on Density Wave Oscillations, focusing on the analysis of the operational parameter effect in the system stability and characteristics of the oscillations. As a result of this investigation, the Ishii-Zuber plane is found to be appropriate to represent the system stability and that the Guido's criteria cannot be used to estimate the instability threshold. Moreover, the oscillation amplitude monotonically increases by increasing the heat flux until it reaches an asymptote and the period is found to decrease when the amplitude is increased. Finally, a new dimensionless correlation based on amplitude ratio, is proposed as a result of the observed trends. It is found to be very useful, not only correlates well the collected data at the onset of Density Wave Oscillation, but also predicts the maximum amplitude for the given sets of operating conditions.

CONTENTS

ABSTRACT.....	vi
CONTENTS.....	viii
LIST OF FIGURES	xii
LIST OF TABLES	xvi
NOMENCLATURE.....	xviii
CHAPTER 1	22
1.1. Motivation	22
1.2. Objective	23
1.3. Scope	23
1.4. Outline	23
CHAPTER 2	24
2.1. Two-Phase Flow Principles.....	24
2.2. Two-Phase Flow Models.....	29
CHAPTER 3	30
3.1. Introduction	30
3.2. Mechanisms of Density Wave Oscillations.....	31
3.3. System Stability.....	32
3.3.1. Stability maps	33
3.3.2. Ishii-Zuber plane.....	38
3.3.3. Stability boundary.....	42

3.4. Parametric effect in System Stability.....	43
CHAPTER 4.....	54
4.1. Experimental Facility.....	54
4.1.1. Pump.....	54
4.1.2. Conditioner.....	54
4.1.3. Heated Section.....	56
4.1.4. Visualization Glass.....	56
4.1.5. Flow Restrictions.....	57
4.1.6. Condenser.....	57
4.1.7. Loop Instrumentation and Uncertainties.....	58
4.1.8. Software Interface.....	59
4.2. Experimental Procedure.....	60
CHAPTER 5.....	63
5.1. Stability Boundaries.....	63
5.1.1. Constant Mass Flux.....	63
5.1.2. Constant heat flux.....	67
5.1.3. Experimental and Theoretical Threshold Lines.....	69
5.2. Oscillation Amplitude.....	70
5.2.1. Parametrical analysis.....	70
5.2.2. Amplitude Correlation.....	73
5.3. Oscillation Period.....	78
5.4. Boundaries of the Experimental Data.....	81
5.4.1. Upper Boundary.....	81
5.4.2. Lower Boundary.....	81
CHAPTER 6.....	84
CHAPTER 7.....	85

REFERENCES.....86

LIST OF FIGURES

- Figure 3.1: Simplified system for Density Wave Oscillations
- Figure 3.2: Stability map of Boure and Mikaila [Aldridge and Fowler, 1996]
- Figure 3.3: Stability map of Ishii and Zuber [Aldridge and Fowler, 1996]
- Figure 3.4: Stability map of Saha et al. [Aldridge and Fowler, 1996]
- Figure 3.5: Stability map of Fowler [Aldridge and Fowler, 1996]
- Figure 3.6: Stability map of Achard et al. when gravity is neglected [Aldridge and Fowler, 1996]
- Figure 3.7: Stability map of Dykhuizen et al. [Aldridge and Fowler, 1996]
- Figure 3.8: Stability map of Rizwan-Uddin and Dorning [Aldridge and Fowler, 1996]
- Figure 3.9: Stability map [Boure et al., 1973]
- Figure 3.10: Oscillatory behavior: (a) Convergent oscillation (b) Divergent oscillation [Belblidia and Bratianu, 1979]
- Figure 4.1: Process and instrumentation diagram of the experimental facility [Ruspini, 2012]
- Figure 4.2: Simplified scheme of the experimental facility
- Figure 4.3: Heated section sketch
- Figure 4.4: Software interface – LabVIEW
- Figure 4.5: Density Wave Oscillation. $m'' = 300$ [kg/m²-s]; $P_i = 700$ [kPa]; $T_i = 278,2$ [K]; $q'' = 48$ [kW/m²]; $K_i \approx 24$; and $K_e \approx 5,6$
- Figure 5.1: Transition from stable to unstable system. $m'' = 210$ [kg/m²-s]; $P_i = 700$ [kPa]; $T_i = 291,2$ [K]; $q'' = 25$ [kW/m²]; $K_i \approx 24$ [-]; and $K_e \approx 5,6$ [-].
- Figure 5.2: Stability boundaries at different mass fluxes. $P_i = 700$ [kPa]; $K_i \approx 24$ [-]; and $K_e \approx 5,6$ [-].
- Figure 5.3: Limiting heat flux as function of inlet subcooling for different mass fluxes. $P_i = 700$ [kPa]; $K_i \approx 24$ [-]; and $K_e \approx 5,6$ [-].

Figure 5.4: Stability boundaries at different heat fluxes. $P_i = 700$ [kPa]; $K_i \approx 24$ [-]; and $K_e \approx 5,6$ [-].

Figure 5.5: Limiting mass flux as function of inlet subcooling for different mass fluxes. $P_i = 700$ [kPa]; $K_i \approx 24$ [-]; and $K_e \approx 5,6$ [-].

Figure 5.6: Comparison between the stability boundary predicted by Guido's equation and the experimental stability boundary. $P_i = 700$ [kPa]; $K_i \approx 24$ [-]; and $K_e \approx 5,6$ [-].

Figure 5.7: Amplitude variation with the heat flux in the Density Wave Oscillations' region at different inlet subcoolings. (\wedge) stands for data taken at $m'' = 300$ [kg/m²-s] and (\vee) stands for data taken at $m'' = 210$ [kg/m²-s]. $P_i = 700$ [kPa]; $K_i \approx 24$ [-]; and $K_e \approx 5,6$ [-].

Figure 5.8: Length of the single-phase region as a function of heat flux for different inlet subcoolings. (\wedge) stands for data taken at $m'' = 300$ [kg/m²-s] and (\vee) stands for data taken at $m'' = 210$ [kg/m²-s]. $P_i = 700$ [kPa]; $K_i \approx 24$ [-]; and $K_e \approx 5,6$ [-].

Figure 5.9: Amplitude variation with the normalized Phase Change number in the Density Wave Oscillations' region at different inlet subcoolings. $m'' = 300$ [kg/m²-s]; $P_i = 700$ [kPa]; $K_i \approx 24$ [-]; and $K_e \approx 5,6$ [-].

Figure 5.10: Void fraction as a function of flowing quality using the Smith's equation as slip ratio

Figure 5.11: Amplitude variation with the Phase Change number at different inlet subcoolings and correlation curves. $m'' = 300$ [kg/m²-s]; $P_i = 700$ [kPa]; $K_i \approx 24$ [-]; and $K_e \approx 5,6$ [-].

Figure 5.12: Amplitude variation with the Phase Change number at different inlet subcoolings and correlation curves. $m'' = 210$ [kg/m²-s]; $P_i = 700$ [kPa]; $K_i \approx 24$ [-]; and $K_e \approx 5,6$ [-].

Figure 5.13: Prediction of the maximum amplitude at different inlet subcoolings. $m'' = 300$ [kg/m²-s]; $P_i = 700$ [kPa]; $K_i \approx 24$ [-]; and $K_e \approx 5,6$ [-].

Figure 5.14: Prediction of the maximum amplitude at different inlet subcoolings. $m'' = 210$ [kg/m²-s]; $P_i = 700$ [kPa]; $K_i \approx 24$ [-]; and $K_e \approx 5,6$ [-].

Figure 5.15: Period variation with the heat flux in the Density Wave Oscillations' region at different inlet subcoolings. (\wedge) stands for data taken at $m'' = 300$ [kg/m²-s] and (\vee) stands for data taken at $m'' = 210$ [kg/m²-s]. $P_i = 700$ [kPa]; $K_i \approx 24$ [-]; and $K_e \approx 5,6$ [-].

Figure 5.16: Effect of the inlet subcooling on the oscillation period at different heat fluxes and mass fluxes. (\wedge) stands for data taken at $m'' = 300$ [kg/m²-s] and (\vee) stands for data taken at $m'' = 210$ [kg/m²-s]. $P_{inlet} = 700$ [kPa]; $K_i \approx 24$ [-]; and $K_e \approx 5,6$ [-].

Figure 5.17: Oscillation period as a function of the single-phase residence time for different inlet subcoolings. (\wedge) stands for data taken at $m'' = 300$ [kg/m²-s] and (\vee) stands for data taken at $m'' = 210$ [kg/m²-s]. $P_i = 700$ [kPa]; $K_i \approx 24$ [-]; and $K_e \approx 5,6$ [-].

Figure 5.18: Typical traces at high inlet subcooling values when the facility thermal limitation is reached before observing Density Wave Oscillations. $m'' = 175$ [kg/m²-s]; $P_i = 695$ [kPa]; $T_i = 273,8$ [K]; $q'' = 32$ [kW/m²]; $K_i \approx 24$ [-]; $K_e \approx 5,6$ [-]; and $T_o = 378,9$ [K].

Figure 5.19: Typical traces of instability found at low inlet subcooling. $m'' = 175$ [kg/m²-s]; $P_i = 695$ [kPa]; $T_i = 293,1$ [K]; $q'' = 32$ [kW/m²]; $K_i \approx 24$ [-]; $K_e \approx 5,6$ [-];

LIST OF TABLES

Table 3.1: Experimental researches of Density Wave Oscillations in boiling systems

Table 4.1: Accuracy relative to the facility instrumentation

Table 4.2: Uncertainties of the main operational parameters

NOMENCLATURE

Variables and Parameters

A	Cross sectional area [m ²]
$A_{\%}$	Amplitude percentage [-]
A_{p-p}	Amplitude peak-to-peak [kg/s]
D	Diameter [m]
e	Entrainment liquid fraction [-]
f_m	Two-phase flow friction factor [-]
h	Enthalpy [J/kg]
h^*	Dimensionless enthalpy [-]
j	Drift velocity [m/s]
K	Resistance coefficient [-]
L	Length of the channel [m]
\dot{m}	Mass flow rate [kg/s]
m''	Mass flux [kg/m ² -s]
N_D	Drift number [-]
N_{pch}	Phase Change number [-]
N_{sub}	Subcooling number [-]
P	Pressure [Pa]
q	Heat input [W]
q'	Heat per unit length [W/m]

q''	Heat flux [W/m^2]
\dot{Q}	Volumetric flow rate [m^3/s]
Re	Reynolds number [-]
S	Slip ratio [-]
t	Time [s]
T	Temperature [K]
u	Velocity [m/s]
v^*	Dimensionless velocity [-]
x	Quality [-]
z	Distance from the entrance [m]
ΔP	Pressure drop [Pa]
ΔT_{sub}	Inlet subcooling [K]

Greek Letters

α	Void fraction [-]
β	Volumetric fraction [-]
γ	Dimensionless exit quality [-]
ε	Friction parameter [-]
μ	Viscosity [Pa-s]
λ	Length of the single-phase region [m]
A	Empirical parameter [-]
ζ	Heated perimeter [m]
ρ	Density [kg/m^3]
τ	Residence time [s]
τ_o	Dimensionless subcooling [-]
Ω	Characteristic frequency [s^{-1}]

Subscripts

<i>e</i>	Exit
<i>eq</i>	Equilibrium
<i>E</i>	Exit reservoir
<i>Ext</i>	External
<i>g</i>	Gas
<i>h</i>	Hydraulic
<i>i</i>	Inlet
<i>I</i>	Inlet reservoir
<i>Int</i>	Internal
<i>j</i>	Drift
<i>l</i>	Liquid
<i>m</i>	Mixture
<i>o</i>	Outlet
<i>R</i>	Reference
<i>s</i>	Superficial
<i>sat</i>	Saturation
<i>sp</i>	Single-phase

CHAPTER 1

INTRODUCTION

1.1. Motivation

The worldwide population growth and the living standard rising in the developing nations have driven the accelerated expansion of the energy consumption in the last decades. In order to satisfy the growing energy demand, the world has become more energy efficient by optimizing the energy utilization, which in many cases is related with finding better solutions for the energy transfer problems. In this sense, the boiling flow systems has shown to be very useful in situations where high heat fluxes are expected, due to the favorable heat transfer characteristics found in such systems [Yuncu et al., 1991].

However, evaporating two-phase flow systems are susceptible to thermo-hydraulic instabilities. Among them, the so-called Density Wave Oscillations are the most common type of thermally induced instability encountered in industrial equipment such as boiling water reactors, boilers, thermosiphons, heat exchangers, chemical reactors and some other chemical process units [Ding et al., 1995].

Such phenomenon, characterized as self-sustained periodic oscillations with periods around twice the particle residence time, may lead to a substantial deterioration of the heat transfer characteristic; decreasing, in that way, the efficiency of the heat transfer process. In addition, the oscillation in the mass flow, system pressure and wall temperature can cause control problems, mechanical vibrations and thermal fatigue; yielding a reduction in the life span of such equipment where this instability may appear [Komakli et al., 2002].

Since Stenning introduced the term Density Wave Oscillations in 1964, several investigations have been done for understanding this phenomenon. In fact, this is definitely the most studied type of two-phase flow instability. Excellent literature reviews on Density Wave Oscillations are given by Boure et al. [1973], Belblidia and Bratianu [1979], Kakac and Bon [2008] and Ruspini [2012].

Upon reviewing the literature, it is clear that most of the researches, either experimental or theoretical, have been focused on vertical systems. Among these, the pioneer investigation performed by Ishii and Zuber [1970] provides a suitable way for analyzing the system stability by development of stability maps based on the dimensionless Phase Change number (N_{pch}) and Subcooling number (N_{sub}). These parameters gather the most relevant information for boiling systems and they are very useful for defining the stable and unstable operating conditions.

But, despite the appropriate system characterization provided by these maps, the literature shows that such stability analyzes are not found for horizontal boiling flows. Moreover, the importance of this kind of research should not be ignored since horizontal systems are encountered more often than vertical systems in the industrial applications [Ding et al., 1995; Komakli et al., 2002].

1.2. Objective

The main aim of present research is to perform an experimental investigation on Density Wave Oscillations, focusing on the analysis of the operational parameter effect in the system stability and characteristics of the oscillations.

1.3. Scope

Density Wave Oscillations will be studied in a horizontal single boiling channel using R-134a (1,1,1,2-tetrafluorethane) as working fluid. The experiments will be performed at constant inlet pressure ($P_i = 700$ [kPa]) and fixed positions of the inlet and exit flow restrictions ($K_i \approx 24$ and $K_e \approx 5,6$). The heat over the boiling channel will be uniformly distributed. The analysis will be performed at 5 levels of inlet subcooling, 2 levels of mass flux and 2 levels of heat flux.

1.4. Outline

In addition to the present chapter, the remaining of this thesis is divided into 6 chapters. The definition of the key parameters and a brief description of the models in two-phase flow is presented in Chapter 2. Then, a discussion about the mechanism and an stability analysis of the Density Wave Oscillations is given in Chapter 3. The experimental setup is introduced and explained in Chapter 4, besides the description of the experimental procedure. Finally, Chapter 5 presents the results of the experimental research, together with an appropriate discussion regarding the trends shown in the literature. The last two chapters contain the conclusion of the present work and recommendations for futures investigations within this topic.

CHAPTER 2

FUNDAMENTALS

This chapter focuses on the key parameters used to describe and analyze the two-phase flow systems. In addition, a brief description of the two phase flow models is given.

2.1. Two-Phase Flow Principles

The two-phase flow phenomenon is regarded as the simplest multiphase flow, where the two phases are chemically identical and only differ in the state of aggregation. The analysis of such systems becomes much more difficult when phase transition take place, inducing a mass transfer at the interface.

Convective and diffusive condensation and vaporization process vary in space and time. A simplifying assumption to these phenomena, where there is coupled mass, momentum and heat transfer, is described the system as an averaged one dimensional flow.

The mass is conserved in the control volume. Thus, the total mass flow rate is the sum of the liquid and gas mass flow rates:

$$\dot{m} = \dot{m}_l + \dot{m}_g \quad (2.1)$$

where \dot{m} [kg/s], \dot{m}_l [kg/s] and \dot{m}_g [kg/s] are the total, liquid and gas mass flow rate, respectively. A standard parameter that accounts for a wide range of mass flow rates and is easier to measure is the mass flux, which is defined as the ratio of the total mass flow rate to the cross sectional area:

$$m'' = \frac{\dot{m}}{A} \quad (2.2)$$

where m'' [kg/m²-s] is the mass flux; and A [m²] is the cross sectional area.

Whenever the system is in saturation state, gas and liquid are the coexisting phases. It is often important to determine the relative proportion of the phases in the system under study. For this purpose, by assuming thermal equilibrium between phases, the so-called static quality is a dimensionless quantity and is defined as the ratio of mass of gas to the the total mass of the system. Likewise, for a fluid flow system, it is assumed that thermal equilibrium between the phases is preserved, and the quality is defined in terms of the flow rates as follows:

$$x = \frac{\dot{m}_g}{\dot{m}} = \frac{\dot{m}_g}{\dot{m}_l + \dot{m}_g} \quad (2.3)$$

where x [-] is called flow quality. Though the quality obtained from mass flow rate ratio is a widely used definition of quality for fluid flows, when phase change occurs the amount of gas flowing through the system changes depending on the heat transfer between the system and the surroundings. Thermodynamic consistency indicates that for a two phase mixture in thermodynamic equilibrium, where the saturated vapor is in equilibrium with the saturated liquid, the quality can be obtained from any of thermodynamic intensive properties, either volumetric or energetic, through the lever rule. Thus, for a control volume is possible to calculate an approximated quality value by assuming thermal equilibrium between the two flowing phases, as follows:

$$x_{eq} = \frac{h_m(z) - h_l}{h_{lg}} \quad (2.4)$$

where x_{eq} [-] is the thermodynamic equilibrium quality; h_l [J/kg] is the saturated liquid enthalpy; h_{lg} [J/kg] is the latent heat of vaporization at the system temperature and pressure; and $h_m(z)$ [J/kg] is the mixture enthalpy at the cross sectional located at a distance z from the entrance, which can be determined by:

$$h_m(z) = h_l + \frac{1}{\dot{m}} \int_0^z q'(z) dz \quad (2.5)$$

where h_i [kJ/kg] is the enthalpy at the inlet of the conduit; and $q'(z)$ [W/m] is the heat transferred to (or from) the system per unit length. It should be noticed that the flow quality and the thermal equilibrium quality are equal if thermal equilibrium exists within the system.

Similarly to the equation for the total mass flow rate, the total volumetric flow rate is the sum of the liquid and gas volumetric flow rates, and this is represented as:

$$\dot{Q} = \dot{Q}_l + \dot{Q}_g \quad (2.6)$$

where \dot{Q} [m³/s], \dot{Q}_l [m³/s] and \dot{Q}_g [m³/s] are the total, liquid and gas volumetric flow, respectively.

Moreover, it can be defined a dimensionless quantity based on the volumetric flow rates, as can be seen in equation 1.7:

$$\beta = \frac{\dot{Q}_g}{\dot{Q}} = \frac{\dot{Q}_g}{\dot{Q}_l + \dot{Q}_g} \quad (2.7)$$

where β [-] is the volumetric fraction, which is related with flow quality through the following relation:

$$\beta = \frac{\frac{x}{\rho_g}}{\frac{x}{\rho_g} + \frac{1-x}{\rho_l}} = \frac{1}{1 + \frac{\rho_g}{\rho_l} \left(\frac{1-x}{x} \right)} \quad (2.8)$$

where ρ_g [kg/m³] and ρ_l [kg/m³] are the gas and liquid densities, respectively.

The void fraction may be regarded as a volumetric fraction of gas in the system. This parameter is considered one of the most important in two-phase flow analyses since it is used to determine the phase velocities; and thus, affect the flow pattern, pressure drop and heat transfer in the system [Moreno, 2005]. The void fraction is then defined in the following way:

$$\alpha = \frac{A_g}{A} = \frac{A_g}{A_l + A_g} \quad (2.9)$$

where α [-] is the void fraction; A_g [m²] is the cross sectional area occupied by void (gas); A_l [-] is the cross sectional area occupied by liquid. It should be notice that the void fraction is a time-space averaged quantity.

As it was stated above, the actual phase velocities depend on the relative cross sectional area occupied by each phase. It represents the true averaged velocity by which each phase is transported. Thus, the actual gas and liquid velocity are defined as follows:

$$u_g = \frac{\dot{Q}_g}{A_g} = \frac{\dot{Q}_g}{\alpha A} \quad (2.10)$$

$$u_l = \frac{\dot{Q}_l}{A_l} = \frac{\dot{Q}_l}{(1 - \alpha)A} \quad (2.11)$$

where u_g [m/s] and u_l [m/s] are the actual gas and liquid velocities, respectively. Also it is possible to define these velocities in terms of the mass flow rates of each phase as follows:

$$u_g = \frac{x \dot{m}}{\alpha \rho_g A} = \frac{x m''}{\alpha \rho_g} \quad (2.12)$$

$$u_l = \frac{1 - x \dot{m}}{1 - \alpha \rho_l A} = \frac{1 - x m''}{1 - \alpha \rho_l} \quad (2.13)$$

It is quite difficult to accurately determine the actual phase velocity due its dependence on the void fraction. Therefore, it is experimentally feasible to determine the superficial velocity instead, which is the average velocity that a phase would have if it would flow alone throughout the total cross sectional area. These superficial velocities are then defined as:

$$u_{sg} = \frac{\dot{Q}_g}{A} = x \frac{m''}{\rho_g} = \alpha u_g \quad (2.14)$$

$$u_{sl} = \frac{\dot{Q}_l}{A} = (1 - x) \frac{m''}{\rho_l} = (1 - \alpha) u_l \quad (2.15)$$

where u_{sg} [m/s] and u_{sl} [m/s] are the superficial gas and liquid velocities, respectively. And the total superficial velocity is given by:

$$u_s = u_{sg} + u_{sl} \quad (2.16)$$

Moreover, sometimes it is useful to define relative velocities between the phases or respect to another reference point. Thus, the drift velocities are defined as the relative motion of the phases in relation to the total superficial velocity. These velocities are stated as:

$$u_{gj} = u_g - u_s \quad (2.17)$$

$$u_{lj} = u_l - u_s \quad (2.18)$$

where u_{gj} [m/s] and u_{lj} [m/s] are the gas and liquid drift velocities, respectively. From these definitions can be also defined volumetric relations called drift fluxes as follows:

$$j_g = \alpha u_{gj} = \alpha(u_g - u_s) \quad (2.19)$$

$$j_l = (1 - \alpha)u_{lj} = (1 - \alpha)(u_l - u_s) \quad (2.20)$$

where j_g [m/s] and j_l [m/s] are the gas and liquid drift fluxes, respectively. In addition, from them own definitions it follows that:

$$j_g + j_l = 0 \quad (2.21)$$

Usually the phases are transported at different velocities. Thus, the ratio between these velocities is known as slip ratio; and this ratio is expressed as follows:

$$S = \frac{u_g}{u_l} \quad (2.22)$$

The slip ratio is typically higher than one, meaning that the actual velocity of the gas phase is greater than the actual liquid velocity; and it is frequently used instead the void fraction. These two parameters give equivalent information about the system and they are related as follows:

$$S = \frac{u_g}{u_l} = \frac{\frac{x m''}{\alpha \rho_g}}{\frac{1 - x m''}{1 - \alpha \rho_l}} = \frac{x(1 - \alpha)\rho_l}{(1 - x)\alpha\rho_g} \quad (2.23)$$

The above equation can be reordered as follows:

$$\alpha = \frac{1}{1 + \left(\frac{\rho_g}{\rho_l}\right) \left(\frac{1 - x}{x}\right) S} \quad (2.24)$$

When the phase velocities are identical, the above equation end up as the equation 1.8; that is, the volumetric fraction is equivalent to the void fraction when the slip ratio is one. Additionally, for this case the mixture density can be defined as:

$$\rho_m = \alpha\rho_g + (1 - \alpha)\rho_l \quad (2.25)$$

2.2. Two-Phase Flow Models

As it was stated earlier, it is common to use one-dimensional models to analyze the two-phase flow systems, mainly due its high complexity. In the literature the most common models are:

- The homogeneous model is widely used due its simplicity. This model assumes the two-phase flow mixture as a pseudo-fluid with no-slip between phases. In such cases when thermodynamic equilibrium is also assumed, this model is called homogeneous equilibrium model.
- The drift-flux model was introduced by Zuber and Findley in 1965 and it is based on the same assumptions that the homogeneous model but allowing velocity difference between the phases;
- The two-fluid model is the most general two-phase flow formulation and it is based in a conservative set of equations for each phase.

CHAPTER 3

DENSITY WAVE OSCILLATIONS

The physical mechanism involved in the occurrence of Density Wave Oscillations (DWO) is introduced in this chapter. Then, an analysis of models used to present and predict the system stability is given. Finally, a review of the operational parameter effects is presented.

3.1. Introduction

According to Kakac and Bon [2008] the study in the two-phase flow field started with the research performed by Lorentz in 1909. Nearly three decades later, in 1938, Ledinegg presented an investigation regarding the thermally induced two-phase flow instabilities, which is considered as the first research in this area. Since then, an enormous amount of researches have been done, mainly due to the big efforts made in the nuclear safety field [Ruspini, 2012].

Nowadays, systems based on convective boiling flows are found in a wide variety of industrial applications, such as boiling water reactors, boilers, thermosiphons, heat exchangers, condenser, chemical reactors and some other chemical process units [Komakli et al., 2002]. Such systems take advantage of the high heat transfer rates that a boiling fluid can reach at moderate temperature differences [Yuncu et al., 1991]. However, those systems are unfortunately susceptible to thermally induced two-phase flow instabilities, such as Ledinegg Instability and Density Wave Oscillations [Boure et al., 1973].

Stenning introduced the term Density Wave Oscillations in 1964 to describe a high frequency oscillatory phenomena which appear in boiling systems due to multiple regenerative feedbacks between the mass flux, void fraction and pressure drop [Boure et al., 1973; Belblidia and Bratianu, 1979]. These oscillations of mass and pressure are totally undesirable, as they can create system control problems, cause mechanical vibration and thermal fatigue of the components, disturb the heat transfer characteristics and induce burnout [Kakac and Bon, 2008].

Finally, it should be mentioned that, most of the researchers state that the Density Wave oscillations are, by far, the most common and studied type of instability in two-phase flow systems, regardless of the fluid and system configuration.

3.2. Mechanisms of Density Wave Oscillations

According to Belblidia and Bratianu [1979] the Density Waves Oscillations can be produced through many different perturbations, being all of them equivalent because this kind of instability is regarded as a fundamental phenomenon. Next, a simple explanation of the mechanisms of Density Wave Oscillation is given.

Consider the system shown in Figure 3.1. This simple model is composed by an inlet and exit reservoir, an inlet and exit flow restriction, a boiling channel (or evaporator) and a heat source. The pressure at the inlet and exit reservoir, P_I and P_E respectively, are kept constant all the time; that is, the system has an externally imposed constant pressure drop. The flow restrictions, where is concentrated the system pressure drop, are located at the inlet and exit of the boiling channel, and these are characterized by the inlet and exit resistance coefficient, K_i and K_e respectively. This dimensionless coefficient is defined as the ratio of the total energy lost over a given segment to the kinetic energy in the section, as show Equation 3.1. Finally, it is assumed that the system operate at steady state condition with a constant heat flux over the channel.

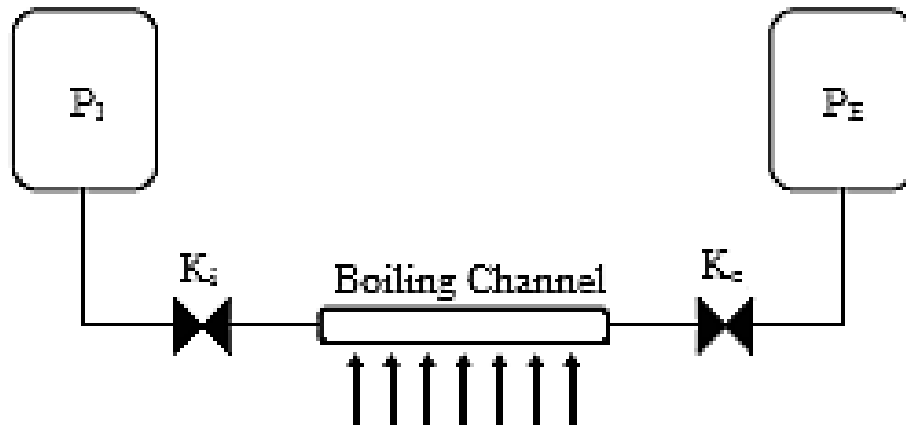


Figure 3.1: Simplified system for Density Wave Oscillations

$$K = \frac{\Delta P}{\frac{1}{2}\rho u^2} \quad (3.1)$$

For the system described shown in Figure 3.1, it is supposed that at time $t = 0$ a positive perturbation of the inlet velocity arises. As at the inlet boiling channel the fluid is a subcooled liquid, the increase in the inlet velocity means an increase in the velocity of the liquid phase. The increase of the liquid phase velocity will cause a reduction of the void fraction, which in practical

terms means an increase in both mixture fluid density and gas phase velocity (see Equations 2.25 and 2.10). At the same time, $t = 0$, this perturbation is sent through channel as a high density wave; and after a time t , which is equal to the residence time of a particle, this wave reaches the exit restriction. The perturbation at the exit restriction will lead to an increase in the exit pressure drop (see Equation 3.1); because the wave has a higher mixture density and velocity with respect to the initial steady state value. But, the system pressure drop is constant; and an increase in the exit pressure drop will cause an instantaneous reduction in the inlet pressure drop to compensate the change. This lower inlet pressure drop will cause a reduction in the inlet velocity (see Equation 3.1); and consequently an increase in the void fraction. Thus, the increased void fraction decreases the average mixture density and gas phase velocity. This new perturbation travels along the channel towards the exit restriction as a low density wave; and once this perturbation reaches the exit restriction, again after a time t , the exit pressure drop will decrease because this new wave has a lower density and velocity than the previous one. The reduction in the exit pressure drop will induce an immediate increase in the inlet pressure drop, to keep constant the total pressure drop in the system; and thus the inlet velocity will increase again. In this way, an oscillation cycle is completed, and the mechanism starts all over again. It should be mentioned that, only for certain combinations of system geometry, operating conditions and boundary conditions the perturbation can acquire the correct timing to become self-sustained [Boure et al., 1973; Belblidia and Bratianu, 1979].

The above explanation of the mechanism is known as the classical description of the Density Wave Oscillations because it suggests that the oscillation period, which is the time needed for a fluid particle for complete a set of event, should be around twice the residence time; and the inlet perturbation must acquire a 180 degrees out-of-phase pressure fluctuation at the exit in order to become a self-sustained periodic oscillation [Boure et al., 1973]. In the literature it is possible to find some similar approaches to the description given, such as in Belblidia and Bratianu [1979] and Kakac and Bon [2008].

3.3. System Stability

In a previous section, it has been highlighted the potential problems triggered by the Density Wave Oscillations in boiling flow systems. Due to those undesirable effects, there is a need to understand and predict such phenomenon.

According to Boure et al. [1973] the stability analysis for Density Wave Oscillations can be done by means of computer codes and simplified models. The computer codes has been mainly developed to handle the complicated mathematics derived from the complex models used in the nuclear safety field; whereas many simplified models have been proposed and used primarily to get a further understanding of this phenomena, and some of them are in good agreement with experimental results.

According to Aldridge and Fowler [1996] the simplified models are mostly given in terms of maps, where can be seen easily the stable and unstable regions. These maps are usually functions of certain dimensionless groups which are useful to reduce the number of independent variables.

3.3.1. Stability maps

Boure and Mikaila [1967] used a homogeneous model to obtain a stability map, which is showed in Figure 3.2, in terms of dimensionless velocity and enthalpy, given by Equations 3.2 and 3.3, respectively.

$$v^* = \frac{\dot{m}}{q} h_R \quad (3.2)$$

$$h^* = \frac{h_l - h_i}{h_R} \quad (3.3)$$

where v^* [-] is the dimensionless velocity; \dot{m} [kg/s] is the mass flow rate; q [W] is the added heat; h_R [J/kg] is a reference enthalpy; h^* [-] is the dimensionless enthalpy; h_l [J/kg] is the saturated liquid enthalpy; and h_i [J/kg] is the enthalpy at the inlet of the channel.

Ishii and Zuber [1970] used a drift-flux model to predict the stability boundary, showed in Figure 2.3, in terms of the dimensionless Phase Change number and Subcooling number, given by Equations 3.4 and 3.5, respectively.

$$N_{pch} = \frac{q}{\dot{m} h_{lg}} \frac{\rho_{lg}}{\rho_g} \quad (3.4)$$

$$N_{sub} = \frac{h_l - h_i}{h_{lg}} \frac{\rho_{lg}}{\rho_g} \quad (3.5)$$

where N_{pch} [-] is the dimensionless Phase Change number; h_{lg} [J/kg] is the latent heat of vaporization; ρ_{lg} [kg/m³] is the density difference between the saturated liquid and gas; ρ_g [kg/m³] is the saturated gas density.

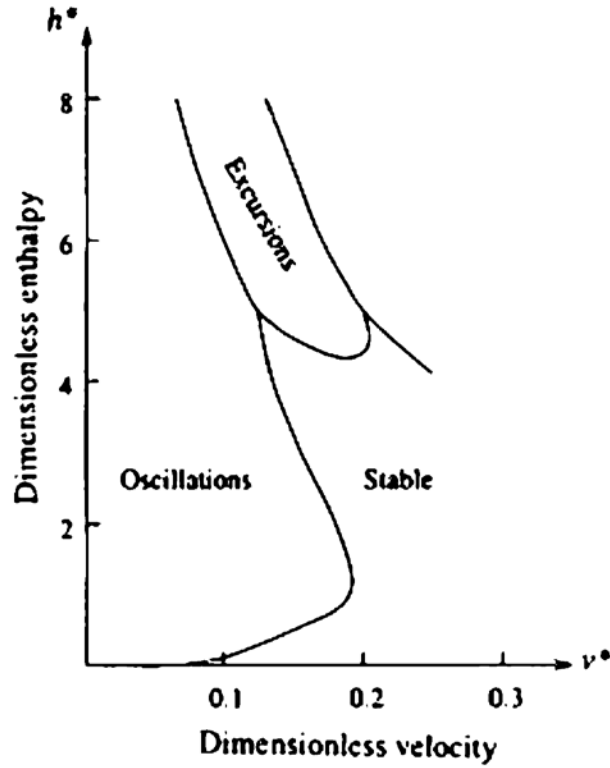


Figure 3.2: Stability map of Boure and Mikaila [Aldridge and Fowler, 1996]

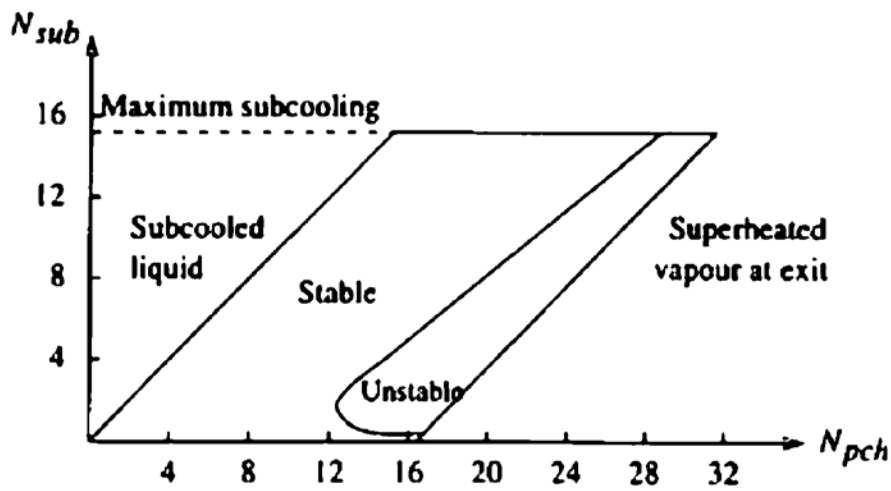


Figure 3.3: Stability map of Ishii and Zuber [Aldridge and Fowler, 1996]

Saha et al. [1976] used a drift-flux model in which a thermal non-equilibrium term was included, to analyze the stability in terms of the dimensionless Phase Change number and Subcooling number, as can be seen in Figure 3.4.

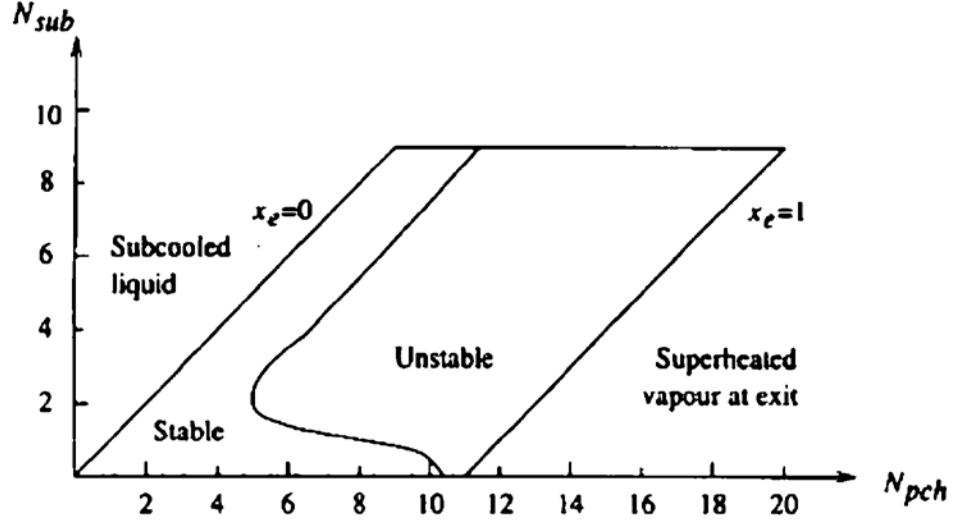


Figure 3.4: Stability map of Saha et al. [Aldridge and Fowler, 1996]

Fowler [1978] derived a stability map using a homogeneous equilibrium model in which the inertial and gravitational terms were neglected. This map has three different curves N , L and S , as can be seen on Figure 3.5. The system is stable below the S curve; oscillatory between S and L ; and static unstable between L and N . This map is presented in terms of dimensionless subcooling and dimensionless exit quality, given by Equations 3.6 and 3.7 respectively.

$$\tau_o = \frac{h_l - h_i}{h_{lg}} \quad (3.6)$$

$$\gamma = \frac{q}{\dot{m}h_{lg}} \quad (3.7)$$

Achard et al. [1980] investigated the stability boundary using a homogeneous equilibrium model in which the effect of friction and gravity were emphasized. This map has two regions, D_0 which is stable and D_2 which is unstable, as can be seen in Figure 3.6. The map was presented in terms of the dimensionless Phase Change number and Subcooling number for the case in which the gravity is neglected.

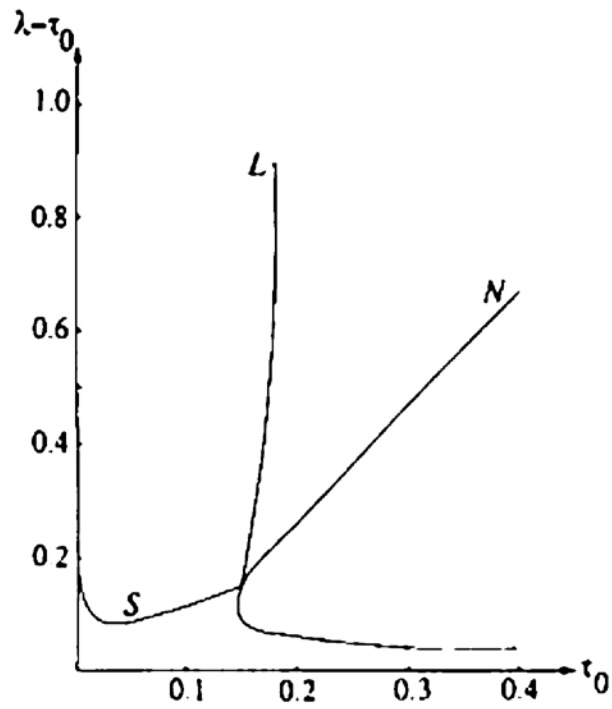


Figure 3.5: Stability map of Fowler [Aldridge and Fowler, 1996]

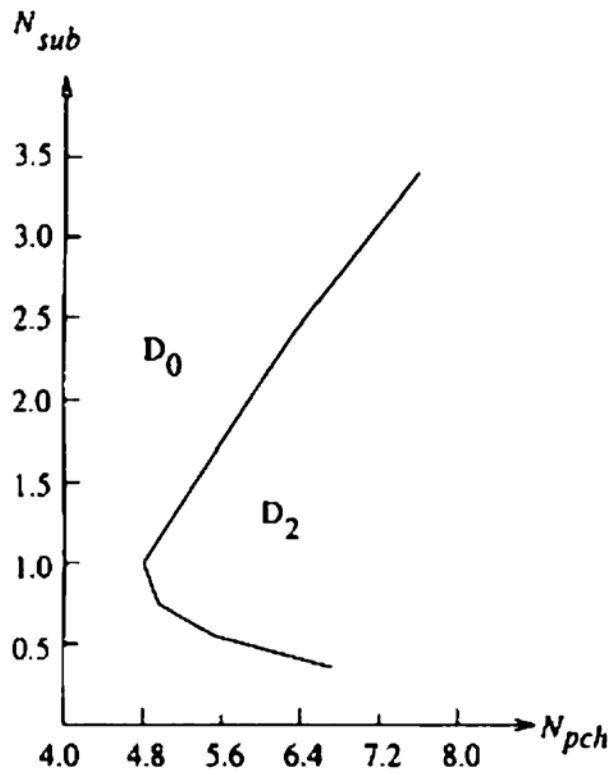


Figure 3.6: Stability map of Achard et al. when gravity is neglected [Aldridge and Fowler, 1996]

Dykhuizen et al. [1986] used a two-fluid model including a thermal non-equilibrium term to predict the stability map in terms of the dimensionless Phase Change number and Subcooling number, as can be seen in Figure 3.7.

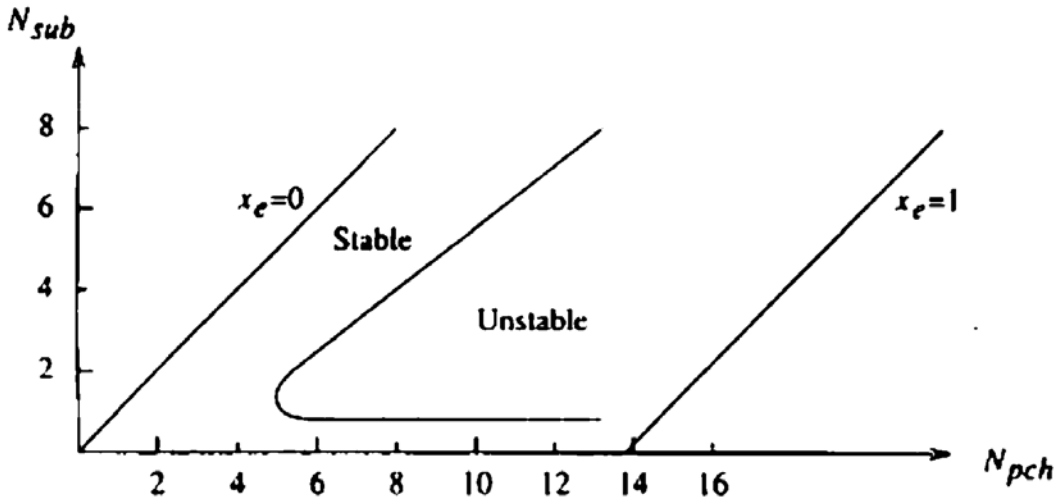


Figure 3.7: Stability map of Dykhuizen et al. [Aldridge and Fowler, 1996]

Rizwan-Uddin and Dorning [1988] used a drift-flux model to generate a stability map in terms of the dimensionless Phase Change number and Subcooling number, as it is shown in Figure 2.8.

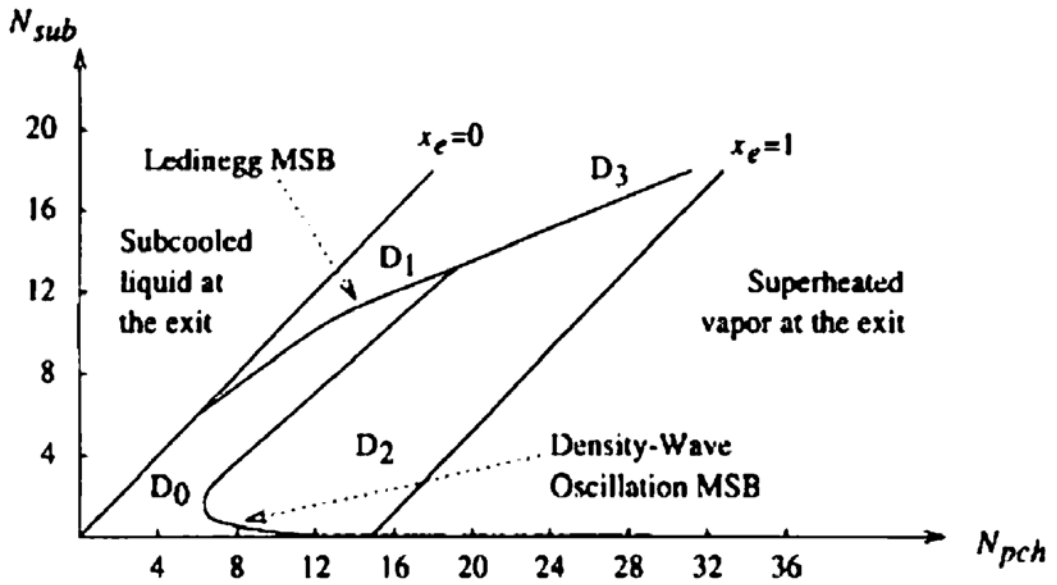


Figure 3.8: Stability map of Rizwan-Uddin and Dorning [Aldridge and Fowler, 1996]

From the analysis showed above, it is clear that the most often used dimensionless numbers in the stability maps are the Phase Change number and the Subcooling number. In this sense, a further discussion of the stability plane proposed by Ishii and Zuber [1970] will be presented in the following section.

3.3.2. Ishii-Zuber plane

The characteristic equation developed by Ishii and Zuber [1970] is used to obtain the appropriate scaling parameters when the system can be assumed in thermodynamic equilibrium. Four dimensionless groups characterize the boiling flow system. Next, these scaling parameters are presented and its significance analyzed.

It is well-known from the basic fluid dynamics that the Reynolds number is one of the most important dimensionless parameters in any fluid flow system, and for the boiling flow case is given by:

$$Re = \frac{\rho_l u_{li} D}{\mu_l} \quad (3.8)$$

where Re [-] is the dimensionless Reynold number; ρ_l [kg/m^3] is the saturated liquid phase density; u_{li} [m/s] is the liquid phase velocity at the inlet of the conduit; D [m] is the conduit diameter; and μ_l [$\text{kg}/\text{m}\cdot\text{s}$] is the dynamic viscosity of the liquid phase. This number provide information concerning to the relative strength between the inertial forces and the viscous forces. Thus, it used to define the flow regime, that is, whether the flow is laminar or turbulent.

An more important dimensionless number that truly characterizes the flow pattern in two-phase flow is known as Drift number, which is given by:

$$N_D = \frac{u_{gj}}{u_{li}} \quad (3.9)$$

where N_D [-] is the dimensionless Drift number; and u_{gj} is the gas drift velocity. This number scales the effect of the relative velocities between the phases.

The dimensionless Phase Change number can be defined as the ratio of the characteristic frequency of phase change to the inverse of particle residence time without any phase change, and this can be expressed in the following way:

$$N_{pch} = \frac{\Omega}{\tau_l^{-1}} \quad (3.10)$$

where Ω [s^{-1}] is the characteristic frequency of phase change; and τ_l [s] is the residence time for the no phase change case. The first term of the above equation scales the rate of phase change due to heat addition in the system; and for the case of thermodynamic equilibrium this is given by:

$$\Omega = \frac{q'' \xi}{\rho_l h_{lg} A} \frac{\rho_{lg}}{\rho_g} \quad (3.11)$$

where q'' [W/m^2] is the heat flux over the wall; ξ [m] is the heated perimeter; and A is the cross sectional area. As for the second term shown in equation 3.10, scales the system residence time of a particle without any heat addition, and this can be written as:

$$\tau_l = \frac{L}{u_{li}} \quad (3.12)$$

where L [m] is the length of the channel. Thus, it can be shown, by doing the algebra, that the definitions presented in equations 3.4 and 3.10 are equivalent. However, the equation 3.10 shows clearly that the Phase Change number can be used as a scaling parameter for time [Saha et al., 1976], since the equality of this number for different systems ensures that the phase change has progressed in the same way in both systems [Ishii and Zuber, 1970].

The last scaling parameter is the Subcooling number, shown in equation 3.5, which scales the inlet subcooling and is regarded as the dimensionless residence time of a particle within the single-phase region under the assumption of thermodynamic equilibrium.

Besides these four dimensionless parameters, the system pressure and the flow restrictions show to be very important for the system stability as well. Nonetheless, in order to present a two dimensional stability map, Ishii and Zuber [1970] chose the Phase Change number and the Subcooling number as the coordinates parameters of such plane, since for a constant system pressure and inlet velocity the Reynolds number, inlet and exit restriction and Drift number are fixed. Furthermore, for a given system pressure the domain of operation is fixed and the stability boundaries can be drawn on this plane for constant velocity and flow restrictions [Ishii and

Zuber, 1970]. An example of such stability map is shown in Figure 3.9, which will be used to explain the most outstanding features that this plane provides.

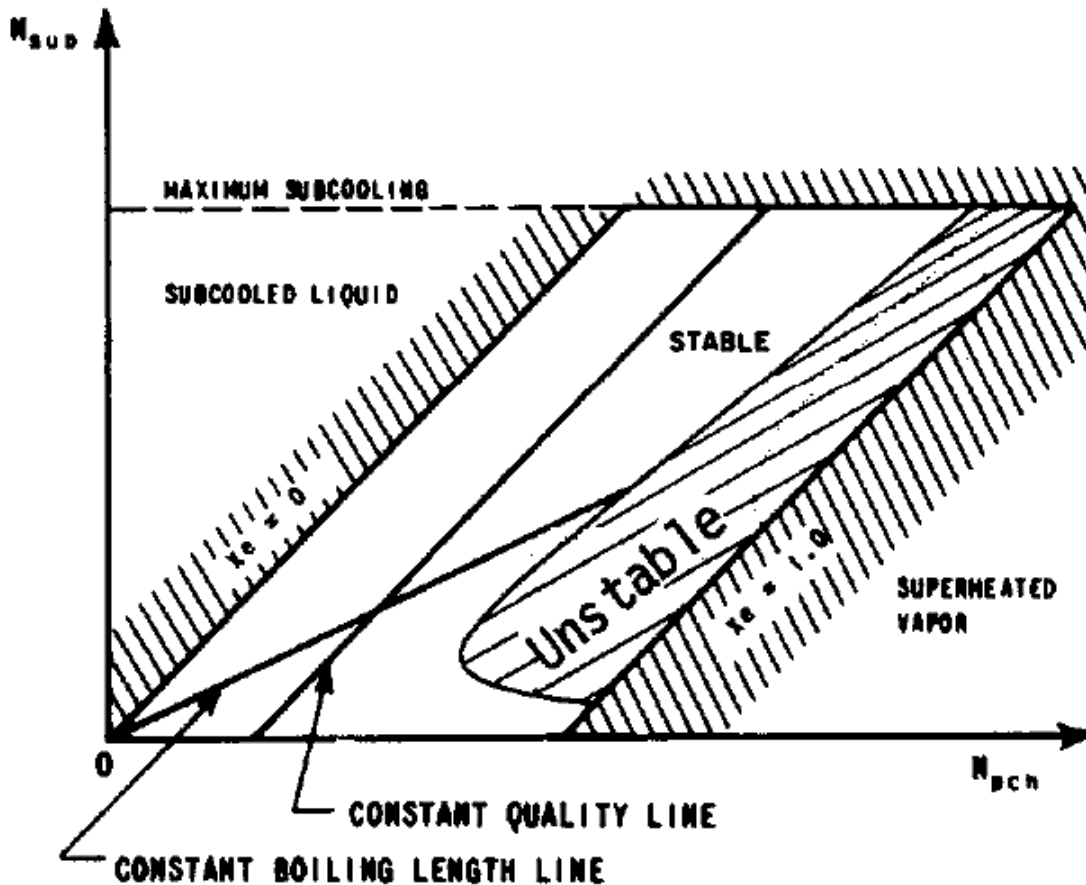


Figure 3.9: Stability map [Boure et al., 1973]

The stability map proposed by Ishii and Zuber [1970] is divided in four main regions below the maximum subcooling level, which is regarded as the maximum subcooling possible for a given system, because over this line there is not fluid but a solid in the channel. In the left hand-side of the map, before the exit equilibrium saturated liquid line ($x_e = 0$), the system yields single-phase liquid flowing throughout the entire boiling channel. Conversely, in the right hand-side, after the exit equilibrium saturated vapor line ($x_e = 1$), the system yields superheated vapor at the channel exit. In the stable two-phase flow region, which is placed between the exit equilibrium saturated liquid line and the stability boundary, if the system is disturbed it will return by itself to its original equilibrium state, as shown in Figure 3.10(a), due to the dominance of the damping effect caused by friction. However, in the unstable region the acceleration and gravity effects prevail and any perturbation in the system will cause a diverging oscillatory behavior, as shown

in Figure 3.10(b). Just on the stability boundary, also called instability threshold and onset of Density Wave Oscillations, self-sustained periodic oscillation with constant amplitude are observed, and they are known as marginally stable oscillations [Belblidia and Bratianu, 1979].

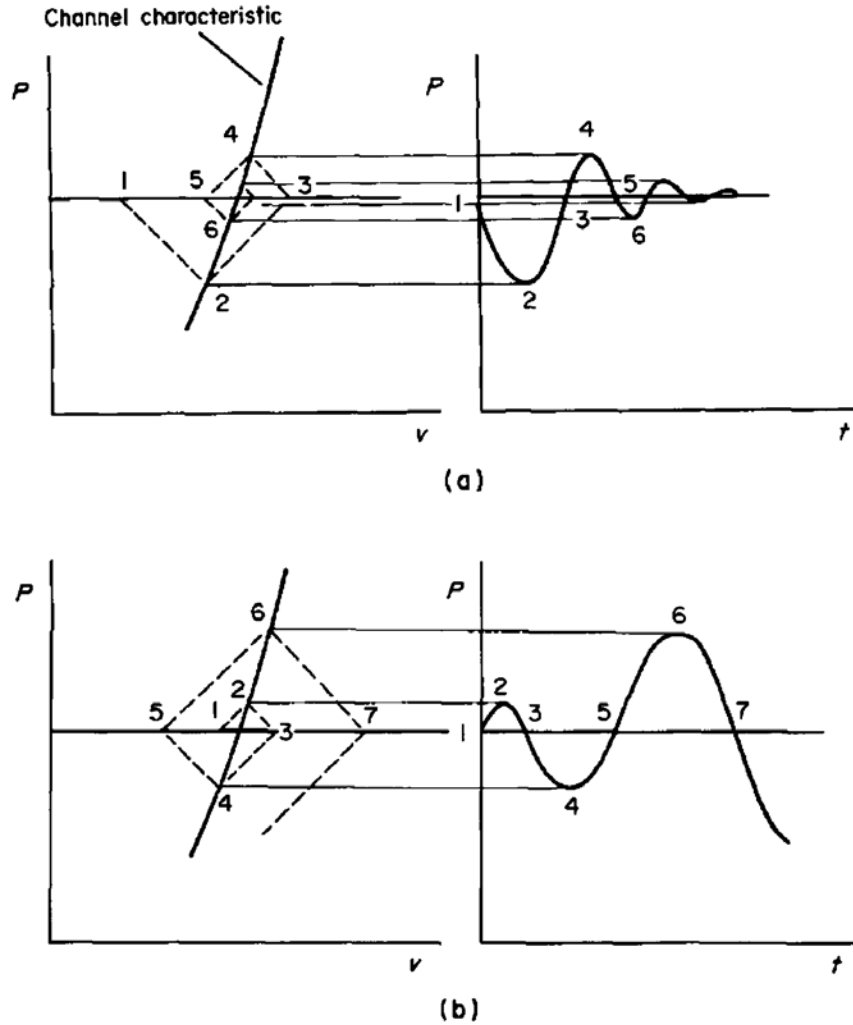


Figure 3.10: Oscillatory behavior: (a) Convergent oscillation (b) Divergent oscillation [Belblidia and Bratianu, 1979]

In addition to the stability boundary, in this plane the boiling boundary ($x_e = 0$) is shown as the first bisectrix, the constant exit quality lines are parallels to the first bisectrix and the constant dimensionless boiling length lines are straight lines through the origin [Boure et al., 1973]. The constant exit quality and dimensionless boiling length lines can be obtained as follows:

$$x_e = (N_{pch} - N_{sub}) \frac{\rho_g}{\rho_{lg}} \quad (3.13)$$

$$\lambda^* = \frac{\lambda}{L} = \frac{N_{sub}}{N_{pch}} \quad (3.14)$$

where λ^* [-] is the dimensionless boiling length; and λ [m] is the length of the non-boiling region or single-phase liquid region. From the equation 3.13 it can be observed that the location of the equilibrium saturated vapor line ($x_e = 1$) is only a function of the system pressure and this line is shifted outwards the boiling boundary as the pressure increases [Saha et al., 1976].

3.3.3. Stability boundary

As it stated in the previous section, the Density Wave Oscillations are normally analyzed in terms of dimensionless stability maps. According to Ruspini [2012] one of the most used stability boundary correlations is the simplified stability criterion of Ishii [1971], which is based on an equilibrium homogeneous model, and is expressed as:

$$N_{pch} = N_{sub} + \frac{2 \left(K_i + \frac{f_m}{2D_h^*} + K_e \right)}{1 + \frac{1}{2} \left(\frac{f_m}{2D_h^*} + 2K_e \right)} \quad (3.15)$$

where f_m [-] is the two-phase flow friction factor; and D_h^* [-] is the dimensionless hydraulic diameter, which is defined as the ratio of channel hydraulic diameter to channel length. This criterion is shown to be valid only for Subcooling numbers larger than the number π ($\pi \approx 3,14159$) [Saha et al., 1976].

However, it is possible to find in the literature models which are valid for all the range of Subcooling numbers such as the Guido's criterion [1991]. This criterion is based on a homogeneous equilibrium two phase flow model assuming that the friction losses are concentrated in the flow restrictions. The expression of this criterion is given as:

$$N_{pch} = N_{sub} + \frac{\varepsilon}{2} \left(1 + \frac{2}{N_{sub}} \right) - \frac{5}{2} + \left\{ \left[\frac{\varepsilon}{2} \left(1 + \frac{2}{N_{sub}} \right) - \frac{5}{2} \right]^2 + \varepsilon \right\}^{\frac{1}{2}} \quad (3.16)$$

where ε [-] is the friction parameter and is given by:

$$\tau = 2 \frac{K_i + K_e}{K_e + 1} \quad (3.17)$$

According to Guido et al. [1991] the best feature of this model is that is able to predict Density Wave Oscillations' thresholds in good agreement with other models.

3.4. Parametric effect in System Stability

This section summarizes the experimentally observed effect of different parameters in the system stability. The parameters considered are:

- Geometry: channel dimensions, flow restrictions, number of channels,
- Operational conditions: pressure, inlet subcooling, mass velocity, power input, type of convection,
- Boundary conditions: axial heat flux distribution, pressure drop across the channel.

Among these parameters, the inlet subcooling is regarded as a very important one for analyzing the system stability. This can be defined as:

$$\Delta T_{sub} = T_{sat} - T_i \quad (3.18)$$

where ΔT_{sub} [K] is the inlet subcooling; T_{sat} [K] is the saturation temperature at the inlet pressure; and T_i [K] is the temperature at the inlet of the channel.

Table 3.1: Experimental researches of Density Wave Oscillations in boiling systems

Year	Author	Fluid	Configuration	Channel	Observations
1955	I. I. Semenovkel	Water	Vertical	Multi	<ul style="list-style-type: none"> • By increasing the inlet pressure drop in the heated channels the system is stabilized.
1956	A. A. Davidov	Water	Vertical	Multi	<ul style="list-style-type: none"> • By increasing the single phase region the system is stabilized. • By increasing the outlet pressure drop the system is destabilized. • The oscillation period is comparable with the residence time of a fluid particle.
1961	G. B. Wallis and J.H. Heasley	Pentane	Vertical	Multi	<ul style="list-style-type: none"> • The increase of the single phase region stabilizes the system, but the increase of the two-phase region destabilizes it.
1965	J. S. Maulbetsh and P. Griffith	Water	Horizontal	Single	<ul style="list-style-type: none"> • The increase of the inlet restriction stabilizes the system, but the increase in the outlet restriction destabilizes it.
1965	V. V. Dolgov and O. A. Sudnitsyn	Water	Vertical	Multi	<ul style="list-style-type: none"> • The decrease of the inlet subcooling reduces the oscillation amplitude. • The increase of the system pressure reduces the oscillation amplitude. • The increase of the inlet pressure drop reduces the oscillation amplitude.

1967	J. D. Crowley et al.	Freon	Vertical	Multi	<ul style="list-style-type: none"> • The increase of the inlet subcooling increases the oscillation amplitude. • The decrease of the heated length stabilizes the system, but has no effect on the oscillation period.
1967	R. P. Mathisen	Water	Vertical	Single	<ul style="list-style-type: none"> • The increase of the inlet subcooling destabilizes the system at low subcooling, but at high subcooling the opposite effect is observed. • The increase of the mass flux stabilizes the system. • Starting a system with high subcoolings can lead to a large amplitude oscillation. • The increase of the system pressure stabilizes the system, but has no effect on the oscillation period. • The decrease of the heated length stabilizes the system.
1969	D. B. Collins and M. Gacesa	Water	Vertical	Multi	<ul style="list-style-type: none"> • The period increases by increasing the mass flux. • The period increases by increasing the heat flux. • The increase of the by-pass ratio destabilizes the system.
1969	G. Yadigaroglu and A. E. Bergles	R-113	Vertical	Single	<ul style="list-style-type: none"> • High order oscillations are found at high subcooling levels. • A cosine heat flux distribution stabilizes the system. • The oscillation period is approximately equal to twice the residence time of a particle fluid.

1971	T. N. Veziroglu and S. S. Lee	R-11	Vertical	Multi	<ul style="list-style-type: none"> • The increase of the inlet pressure drop stabilizes a cross-connected system, but has no effect in a system without cross-connections. • A cross-connected system is more stable than either single channel or parallel channels without cross-connections. • In cross-connected systems the oscillatory flows through the channels are in-phase, but in systems without cross-connections the oscillatory flows are 180 degrees out-of-phase.
1976	J. C. Friedly	Nitrogen	Vertical	Multi	<ul style="list-style-type: none"> • Decrease the inlet to outlet pressure drop ratio destabilizes the system.

1976	P. Saha et al.	R-113	Vertical	Single	<ul style="list-style-type: none"> • As the inlet subcooling increase, the system stability decrease until a certain subcooling, and starts to increase thereafter. • The period increases monotonically with increasing inlet subcooling. • The system stability depends on the mass flux. • The inlet pressure has no effect on the system stability. • As the inlet throttling increase, the system becomes more stable. • The system becomes less stable by increasing the exit restriction only at low subcooling levels. • The period is indeed on the order of the particle residence time. • The system pressure drop and the inlet mass flow have a phase shift between 90 and 180 degrees.
1977	S. Kakac et al.	R-11	Vertical	Multi	<ul style="list-style-type: none"> • The oscillations are in-phase in all the channels, in both systems with and without cross-connections.
1977	T. N. Veziroglu et al.	R-11	Vertical	Single	<ul style="list-style-type: none"> • There is a linear relationship between subcooling level and mass flow rate at the instability threshold line (except for high subcooling).

1979	M. Aritomi et al.	Water	Vertical	Multi	<ul style="list-style-type: none"> • The period is sensitively dependent on the subcooling level. • The increase of the entrance throttling stabilizes the system. • The system is more unstable when the flow conditions are equal in all the channels. • The amplitude ratio tended to augment with increasing departure from the stable boundary into the unstable region.
1981	H. C. Unal	Water	Vertical	Multi	<ul style="list-style-type: none"> • A small amount of inlet throttling does not affect the system stability, but affect the oscillation period.
1983	T. Dogan et al.	R-11	Vertical	Single	<ul style="list-style-type: none"> • The system is unstable close to the saturated vapor state.
1983	A. Mentès et al.	R-11	Vertical	Single	<ul style="list-style-type: none"> • Different heater surface configurations have no effect on the oscillation period.
1985	K. Mishima et al.	Water	Vertical	Single	<ul style="list-style-type: none"> • The flow becomes more unstable by decreasing the inlet throttling. • The flow becomes more unstable by decreasing the bypass. • The flow becomes more unstable by providing upstream compressibility.
1989	A. Mentès et al.	R-11	Vertical	Single	<ul style="list-style-type: none"> • Amplitudes and periods of the oscillations increase by increasing inlet subcooling.

1990	H. Yuncu	R-11	Horizontal	Single	<ul style="list-style-type: none"> • The amplitude of the oscillations increases by increasing the mass flux. • The amplitude of the oscillations increases by increasing the heat flux. • The system is totally independent of the compressible volume.
1991	H. Yuncu et al.	R-11	Horizontal	Single	<ul style="list-style-type: none"> • The amplitude increases by increasing the heat flux, but the period decrease. • The system stability, amplitude and period increase by decreasing exit orifice diameter. .
1991	H. T. Liu and S. Kakac	R-11	Vertical	Single	<ul style="list-style-type: none"> • The oscillations occur at the single phase vapor region.
1993	M. Xiao et al.	Water	Vertical	Multi	<ul style="list-style-type: none"> • Balanced heating gives a more unstable system than an unbalanced heating. • A single channel is more stable than a parallel channel.

1994	Q. Wang et al.	Water	Vertical	Single	<ul style="list-style-type: none"> • At low system pressure, the stability increase monolithically by increasing the subcooling, but at high system pressure the trend shows a minimum. • The oscillation periods increase systematically with the increase of the inlet subcooling. • The increase in the mass flux leads the two-phase flow system to become more stable. • The oscillation amplitude and period decrease by increasing the heat flux. • The system becomes more stable at higher system pressure, and also increase the oscillation periods. • As the outlet orifice diameter decreases, the system becomes less stable and the oscillation periods increase. • The mass flux oscillation is always accompanied by a wall-temperature oscillation.
1994	I. S. Kyung and S. Y. Lee	R-113	Vertical	Single	<ul style="list-style-type: none"> • The system is stabilized by increasing the inlet subcooling. • The system is stabilized by increasing the inlet restriction, and/or decreasing the exit restriction.

1995	Y. Ding et al.	R-11	Horizontal	Single	<ul style="list-style-type: none"> • By decreasing the inlet subcooling the amplitude and period are decreased. • The oscillation amplitudes and periods decrease with a decrease of mass flux. • The amplitude and period decrease by increasing the heat flux. • The oscillations of pressure and mass flux are in phase. • The period is on the order of the particle residence time. • The bottom wall temperature remained almost constant during density wave type oscillations, while the top wall temperature fluctuated to some degree.
2000	J. M. Kim and S. Y. Lee	Water	Vertical	Single	<ul style="list-style-type: none"> • The system is stabilized by increasing the inlet flow resistance, especially at the high heat flux and the high inlet subcooling conditions.
2001	Furuya et al.	Water	Vertical	Single	<ul style="list-style-type: none"> • For low subcoolings, the system stability increase by increasing the heat flux.

2002	S. Karsli et al.	R-11	Horizontal	Single	<ul style="list-style-type: none"> • The system stability increases with increasing inlet subcooling, regardless of the surface tube configurations. • Periods and amplitudes decrease for all heater tube configurations as the mass flow rate is decreased. • Periods and amplitudes change depending on heater tube configurations. • The system stability increases with decreasing equivalent diameter for the same type heater tube configurations.
2004	W. J. M. De Kruijf et al.	R-12	Vertical	Single	<ul style="list-style-type: none"> • For low subcooling values, the system stability increases as the power is increased, when keeping the subcooling constant.
2010	Y. Guo et al	Water	Vertical	Multi	<ul style="list-style-type: none"> • Non-uniform heating makes the system unstable with the increase of non-uniform degree. • The increase of system pressure leads the system to become more stable. • Increasing the inlet resistance coefficient stabilizes the system.
2010	V. Jain et al.	Water	Vertical	Multi	<ul style="list-style-type: none"> • The system stability increase as the system pressure is increased. • The oscillations among the channels are mixed, meaning that is neither in-phase nor out-of-phase. • Channels have slightly different thresholds of instability.
2011	N. Liang et al.	R-22	Horizontal	Single	<ul style="list-style-type: none"> • The instability takes place at almost all the mass velocities.

2012	Z. Deng et al.	Water	Vertical	Multi	<ul style="list-style-type: none"> • The increase of the mass flux increases the stability of the system, but the period and amplitude is decreased. • The increase of the inlet pressure increases the stability of the system.
2012	T. Xiong et al.	Water	Vertical	Multi	<ul style="list-style-type: none"> • The flow becomes more stable by increasing the inlet subcooling. • The flow becomes more stable with increasing the system pressure.

CHAPTER 4

EXPERIMENTAL SYSTEM

The characteristics and components of the experimental setup used in the present research are described in this chapter. Also, the experimental procedure and the uncertainties relative to the measurements are presented.

4.1. Experimental Facility

The experimental facility used in the present research is shown in Figure 4.1. It has been designed and built to generate and investigate both static and dynamic two-phase flow instabilities, using the conditions in the LNG (Liquefied Natural Gas) industry as a reference case. Refrigerant R-134a (1,1,1,2-tetrafluorethane) is used as working fluid due to its low boiling point (312,5 [K] at 1000 [kPa] – 140,5 [K] lower than water), low latent heat of vaporization ($1,6 \cdot 10^5$ [J/kg] at 1000 [kPa] – one order lower than water) and non-flammable characteristic [Ruspini, 2012].

A basic scheme containing the most important components for the Density Wave Oscillations analysis conducted is presented in Figure 4.2. In the following sections each component will be briefly described.

4.1.1. Pump

A gear pump with a magnetic drive coupling (GB-MICROPUMP) is used to circulate the fluid through the loop. This pump allows pressure increase from 400 up to 1000 [kPa]. An interface software is used for controlling the flow rate in the loop; and a PID controller is implemented to keep it constant at the desirable value.

4.1.2. Conditioner

A plate-fin heat exchanger (B8THx14 SWEP) is used to control the inlet temperature of the working fluid at the heated section. This heat exchanger is connected to interface software where the reference temperature can be adjusted.

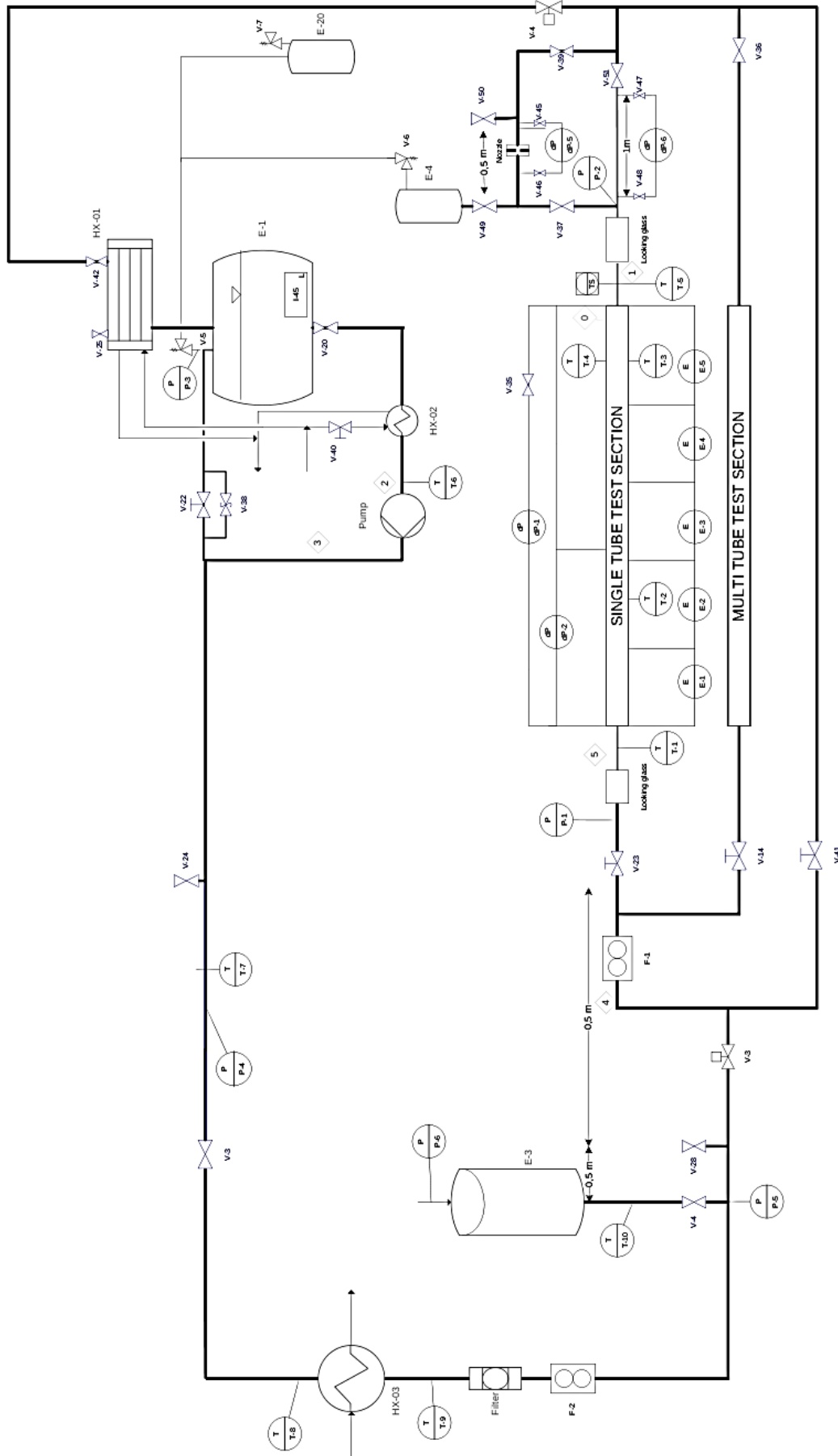


Figure 4.1: Process and instrumentation diagram of the experimental facility [Ruspini, 2012]

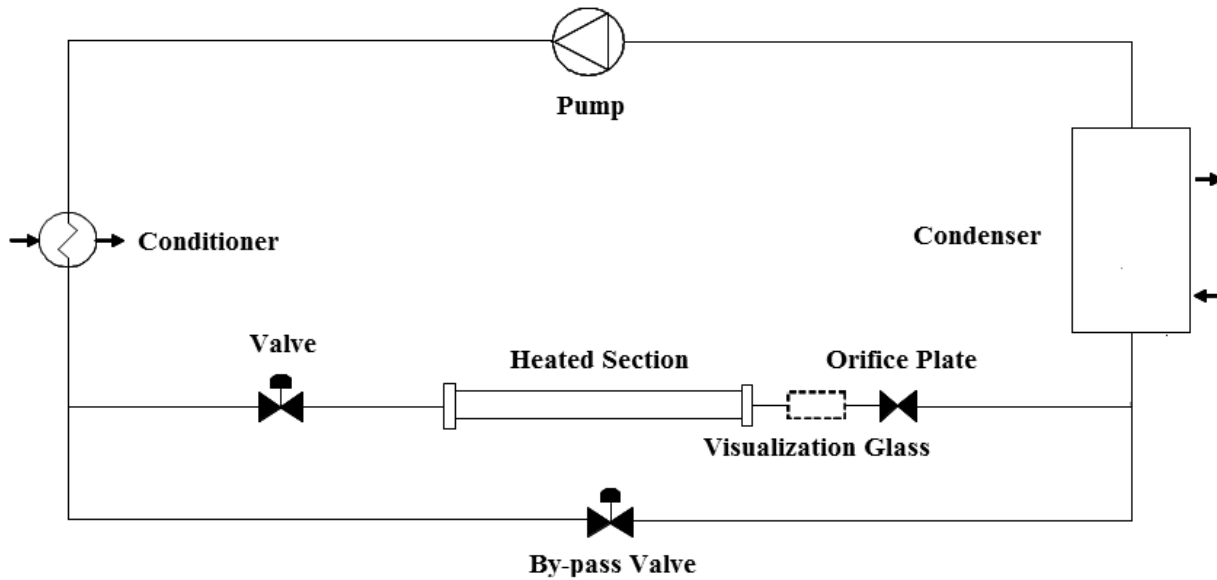


Figure 4.2: Simplified scheme of the experimental facility

4.1.3. Heated Section

It consists in a stainless steel tube of 5 [mm] inner diameter, 8 [mm] outer diameter and 2 [m] long. This section contains 7 pressure taps for differential pressure drop measurements, 12 external thermocouples to measure the wall temperature along the tube, 2 internal thermocouples to study the heat transfer characteristics and 6 electrodes to control the heat distribution. A sketch of the heated section and its components is presented in Figure 4.3.

As can be seen in Figure 4.3, the heated section is divided in 5 segments of 0,4 [m] long to achieve a non-uniform heat profile. Each of these segments is regarded as a heater where the applied power can be specified individually in the interface software up to 500 [W]. Thus, the entire section is heated by Joule effect and is covered by an isolating material to reduce the heat loss with the surroundings. It should be mentioned that, the thermal losses, which are never higher than 8% for any experimental case, are taken into account to calculate the actual heat transferred to the fluid [Ruspini, 2012].

4.1.4. Visualization Glass

A borosilicate tube (fabricated at RealFag, NTNU) is used to perform a photographic analysis of the flow pattern at the outlet of the heated section by using a high speed camera (Photron – FastCam SA3). Moreover, the glass tube acts as a dielectric and thermal insulator between the

heated section and the rest of the loop. The tube is 5 [mm] inner diameter, 8 [mm] outer diameter and 20 [cm] long; and has been designed to uphold up to 2500 [kPa].

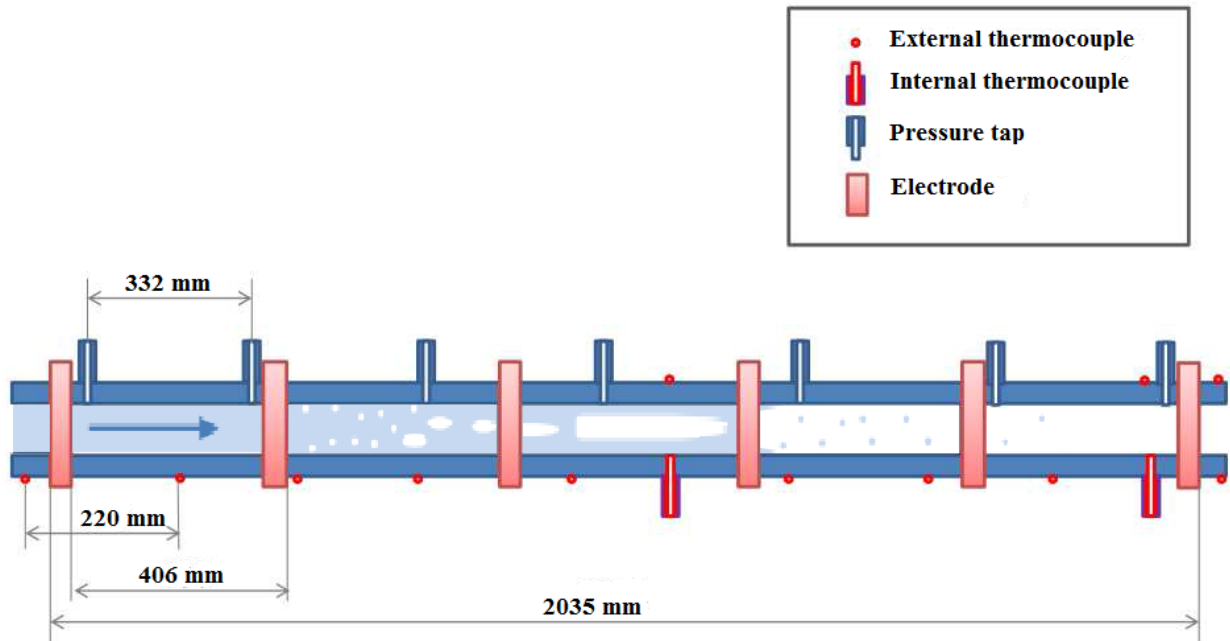


Figure 4.3: Heated section sketch

4.1.5. Flow Restrictions

A valve manually operated provides the local pressure drop at the inlet of the heated section, which is quantified by the inlet resistance coefficient (K_i); whereas for the exit restriction an orifice plate is used, and its pressure drop is measured by the exit resistance coefficient (K_e). This orifice can be modified to analyse the effect of varying local pressure drops at the heated section outlet. Thus, the range of values for the inlet resistance coefficient ranges between 5 and 500; whereas the exit resistance coefficient ranges between 2 and 50. Finally, an adjustable valve is installed in the by-pass branch in order to guarantee the constant pressure drop boundary condition in the heated section [Saha et al., 1976].

4.1.6. Condenser

A shell and tube heat exchanger with a solution of glycol and water in the tube side (CFC-12 – Alpha Laval) is used to condense the working fluid coming from the heated section. It has a capacity of $8 \cdot 10^{-3}$ [m³] and a power input condenser of 1,8 [kW]. This heat exchanger is also connected to the interface software to adjust the reference temperature, which provides the lowest

pressure level in the loop (saturation pressure at the temperature of the working fluid in the condenser).

4.1.7. Loop Instrumentation and Uncertainties

As Shown in Figure 4.1, two coriolis flow meters (Bronkhorst Cori-Tech) are used to measure the volumetric flow before and after the surge tank; absolute pressure transducers (GE-UNIK 5000) are used to measure the pressure in the tanks, after the surge tank, before and after the heated section; differential pressure transducers (Endress+Hauser) are placed in the heated section and flow restrictions; and finally, thermocouples (Standard) are located before and after the conditioner, before the pump, before, after and inside of the heated section. The accuracy of the above instrumentation is presented in Table 4.1. Moreover, Table 4.2 shows the associated error of the main operational parameters in the present research.

Table 4.1: Accuracy relative to the facility instrumentation

Name	Instrument	Range	Measurement Accuracy	Statistical Error
F 1-2	Coriolis Flow Meter	0 - 50 [cm ³ /s]	0,2 [cm ³ /s]	0,2 [cm ³ /s]
P 1-5	Absolute Pressure Transducer	100-1600 [kPa]	10 [kPa]	1 [kPa]
DP1	Differential Pressure Transducer	0 - 100 [kPa]	0,08 [kPa]	0,1 [kPa]
DP2	Differential Pressure Transducer	0 - 100 [kPa]	0,08 [kPa]	0,5 [kPa]
DP3	Differential Pressure Transducer	0 - 100 [kPa]	0,08 [kPa]	0,2 [kPa]
T 1-20	Thermocouple K	223 - 373 [K]	0,1 [K]	0,1 [K]
H 1-5	Heater	0 - 500 [W]	20 [W]	20 [W]

Table 4.2: Uncertainties of the main operational parameters

Name	Symbol	Error
Mass Flux	m''	± 10 [kg/m ² -s]
Inlet Pressure	P_i	± 10 [kPa]
Inlet Temperature	T_i	$\pm 0,2$ [K]
Heat Flux	q''	± 1 [kW/m ²]
Inlet Resistance Coefficient	K_i	± 2 [-]
Exit Resistance Coefficient	K_e	$\pm 0,6$ [-]

4.1.8. Software Interface

The software used to control and monitor the experimental facility is called LabVIEW (Laboratory Virtual Instruments Engineering Workbench). The interface, shown in Figure 4.4, has been designed by Ruspini [2012] and developed by “National Instruments”. The experimental facility is controlled by setting the velocity of the pump, the power over the heated section and the reference temperature in the condenser and conditioner, chillers K6 and K9 respectively. It shows all the measurements provided by the thermocouples, flow meters, heaters, absolute and differential pressure transducers schematically on the interface. Moreover, the main features of this software are:

- Data acquisition
- On-line visualization
- Power control: PID control of the power and heat distribution.
- Pump control: PID control of the flow.
- Chillers control: PID control of the temperatures.
- Alarm control: As a safe system the heat source is shut-down when is reached
 - Maximum temperature: 463 [K]
 - Maximum current: 200 [A]
 - Maximum pressure: 1500 [kPa]

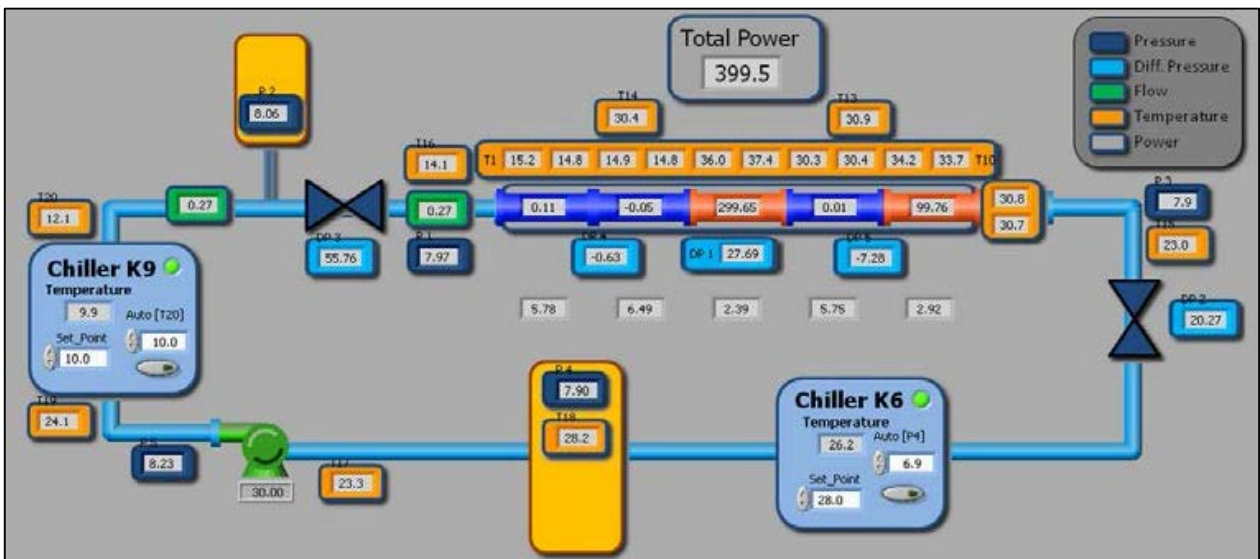


Figure 4.4: Software interface – LabVIEW

4.2. Experimental Procedure

The experiments are conducted in such way that the collected data could be easily presented in the Ishii-Zuber stability map discussed in the previous chapter. During the experiments, the pressure at the inlet of heated channel is kept constant at 700 [kPa]. Also, the configurations of the inlet and exit flow restrictions are set, that is, $K_i \approx 24$ and $K_e \approx 5,6$ for all the experimental runs.

In these experiments, the effect of the inlet temperature, mass flux and heat flux on system stability is analyzed by investigating:

- 5 levels of inlet temperature: 273,2 [K]; 278,2 [K]; 283,2 [K]; 288,2 [K]; and 291,2 [K];
- 2 levels of mass flux: 300 [kg/m²-s]; and 210 [kg/m²-s];
- 2 levels of heat flux: 48 [kW/m²]; and 32 [kW/m²].

The experimental procedure followed in the experiments can be divided in two slightly different methodologies, depending on whether a particular experiment is conducted at constant mass flux or constant heat flux. Next, the common steps for both methodologies are described; then the particular steps for each methodology are presented.

- General steps:

- (1) Check the inlet valve position and the outlet orifice diameter at the heated section.
- (2) Turn on the facility main power, instrumentation and computer.
- (3) Start the interface software (LabVIEW) in the computer.
- (4) Turn on the condenser, conditioner, pump and heaters.

- Constant mass flux:

- (5a) Fix the desired mass flux adjusting the pump velocity in LabVIEW.
- (6a) Fix the desired pressure at the inlet of the heated section adjusting the reference temperature of the condenser in LabVIEW.
- (7a) Set the desired temperature at the inlet of the heated section adjusting the reference temperature of the conditioner in LabVIEW.
- (8a) Start recording the measured variables given by the instrumentation.
- (9a) Increase uniformly the heat flux in LabVIEW by small steps until self-sustained periodic oscillations are observed. It is necessary to allow enough time between successive increments in order to observe the true nature of the system (stable or unstable).

Additionally, it is essential to keep constant the average mass flux, pressure and temperature at the inlet of the heated section throughout the whole data acquisition process.

(10a) Once the instability is recorded for a considerable period of time, decrease completely the heat flux and take the system back to step 7a. Then, repeat steps 8a and 9a.

(11a) Once all the inlet subcooling levels are tested for a given mass flux, take the system back to step 5a and repeat all the steps up to 10a. When the experimental set with the last desired mass flux is completed, finish the experiment by turning off all the facility components.

- Constant heat flux:

(5b) Set the maximum pump velocity in LabVIEW.

(6b) Fix the desired heat flux (uniformly distributed) in LabVIEW.

(7b) Fix the desired pressure at the inlet of the heated section adjusting the reference temperature of the condenser in LabVIEW.

(8b) Set the desired temperature at the inlet of the heated section adjusting the reference temperature of the conditioner in LabVIEW.

(9b) Start recording the measured variables given by the instrumentation.

(10b) Reduce the velocity of the pump by small steps until self-sustained periodic oscillations are observed. It is necessary to allow enough time between successive reductions in order to observe the true nature of the system (stable or unstable). Additionally, it is essential to keep constant the average pressure and temperature at the inlet of the heated section throughout the whole data acquisition process.

(11b) Once the instability is recorded for a considerable period of time, increase to the maximum the pump velocity and take the system back to step 8b. Then, repeat steps 9b and 10b.

(12b) Once all the inlet subcooling levels are tested for a given heat flux, take the system back to step 5b and repeat all the steps up to 11b. When the experimental set with the last desired heat flux is completed, finish the experiment by turning off all the facility components.

According to Belblidia and Bratianu [1979] since the Density Wave Oscillation is regarded fundamental phenomenon, the different ways of generate it are totally equivalents and the chosen way is just a matter of convenience. Regarding this statement, typical traces of the mass flux, inlet pressure, temperatures throughout the heated section and heat flux are shown in Figure 4.5.

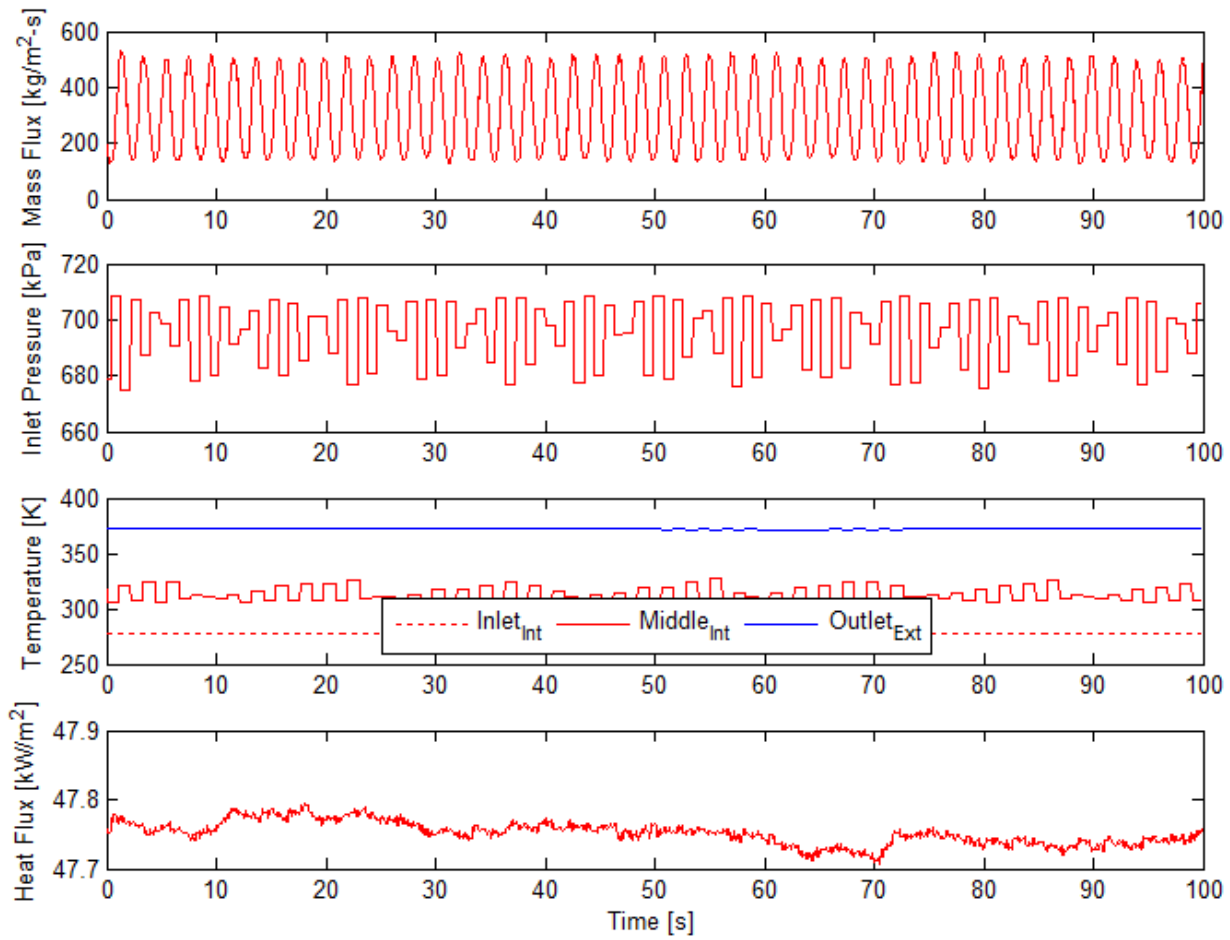


Figure 4.5: Density Wave Oscillation. $\dot{m}'' = 300$ [kg/m²-s]; $P_i = 700$ [kPa]; $T_i = 278,2$ [K];
 $q'' = 48$ [kW/m²]; $K_i \approx 24$; and $K_e \approx 5,6$

CHAPTER 5

RESULTS AND DISCUSSION

The main results of the present research are presented in this chapter. The system stability is experimentally determined at different operational conditions, and the result is compared against the Guido's criterion. The oscillation amplitude is analyzed and new equation is proposed to correlate the experimental data. Finally, the oscillation period is compared with the trends shown in the literature.

5.1. Stability Boundaries

For the experimental determination of the stability boundary, is necessary to define a suitable criteria for establishing whether the system must be considered stable or unstable. However, a general criteria does not exist, and thereby, different researchers use rather different approach to define the exact point where the system becomes unstable. The most used criteria for determination of instability inception are discussed in Saha et al. [1976] and Colombo et al. [2011]. The criteria used in this research is consistent with the criteria used by Colombo et al. [2011], where the system can be considered unstable when a self-sustained periodic oscillation with constant amplitude appears, regardless of the actual size of the oscillation amplitude. In the following sections, experimental stability maps will be presented for the different operational conditions studied in this work; and thereafter, a brief comparison between this results and the prediction provided by the simplified model proposed by Guido et al. [1991] will be given.

5.1.1. Constant Mass Flux

The transition from stable (non-oscillatory) to unstable system can be seen in Figure 5.1. This figure shows that a small increment in the heat flux (around 2600 [s]) drives the system to the Density Wave Oscillations' region. In such situation, it is said that the system has reached the limiting heat for instability inception for the given geometrical configuration, mass flux, inlet pressure and temperature. This operating condition can be presented in the Ishii-Zuber plane, which report the system stability as function of the dimensionless Phase Change number and Subcooling number (further information is given in Chapter 3).

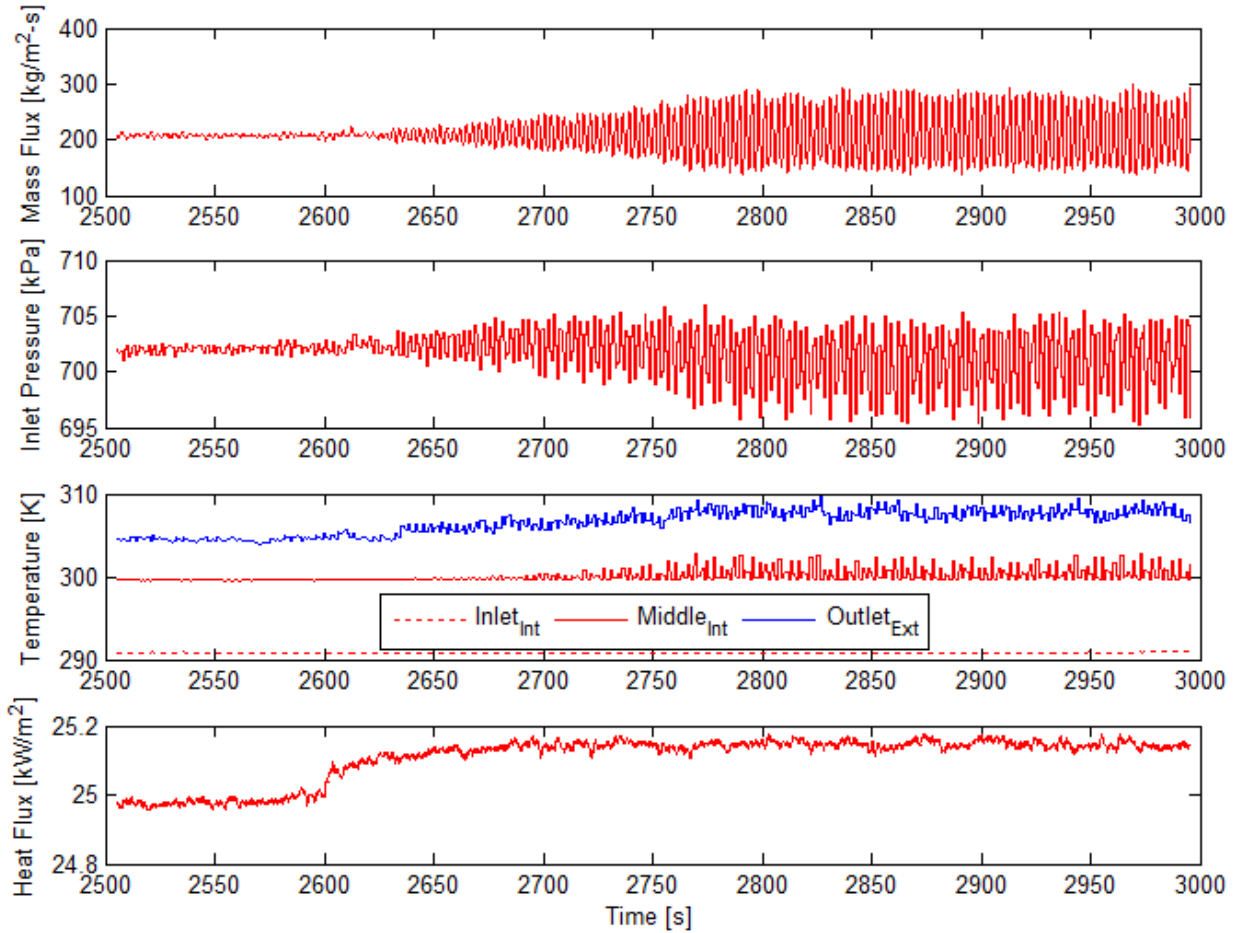


Figure 5.1: Transition from stable to unstable system. $m'' = 210$ [kg/m²-s]; $P_i = 700$ [kPa]; $T_i = 291,2$ [K]; $q'' = 25$ [kW/m²]; $K_i \approx 24$ [-]; and $K_e \approx 5,6$ [-].

The collected inception data for two different mass fluxes is shown in Figure 5.2 on an Ishii-Zuber stability map. Error bars have been included for considering the effects of the measured variables' uncertainties on the dimensionless numbers' computation. The uncertainties of these secondary variables have been estimated based on linear propagation techniques [Moffat, 1988], using the errors presented in Table 4.2. For the Phase Change number (N_{pch}), the effects of mass flux and heat flux uncertainties have been included in the error bars; and similarly, the effect of the inlet temperature uncertainty has been considered in the Subcooling number (N_{sub}); however, this effect cannot be appreciated in Figure 4.2 because it can be considered to be too small ($N_{sub} \pm 0,05$), as the Subcooling number ranges between 2,40 [-] and 7,10 [-]. It should be mentioned that, the effect of the inlet pressure was not considered because this parameter remains constant ($P_i = 700$ [kPa]) for all the experimental sets, likewise the flow resistance coefficients ($K_i \approx 24$ [-] and $K_e \approx 5,6$ [-]).

The stability boundary for the two different mass fluxes ($m'' = 300$ [kg/m²-s] and 210 [kg/m²-s]) analyzed in the present research are shown in Figure 5.2. These curves are practically overlapped, what is similar to the findings reported by Saha et al. [1976] and Colombo et al. [2011]. This result effectually means that, the dimensionless Phase Change number is a well-suited parameter to represent the system stability; since once the geometrical configuration and inlet conditions are established, the input heat to mass flow rate ratio (q/\dot{m}) [J/kg] determines the instability threshold [Colombo et al., 2011].

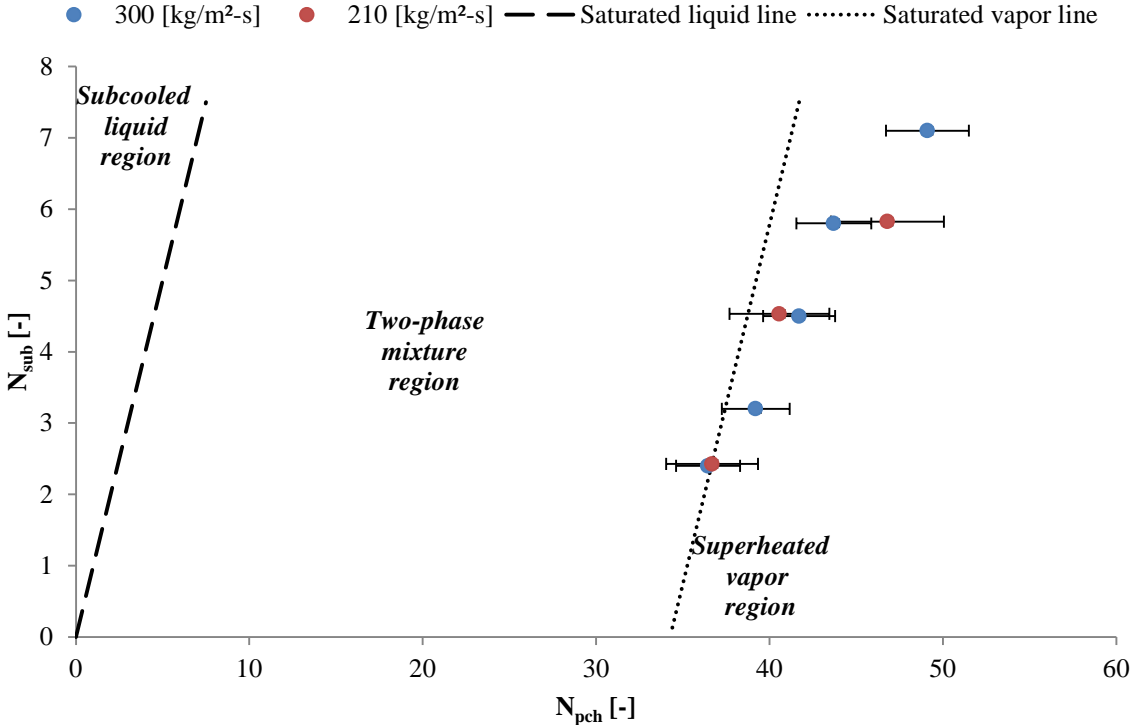


Figure 5.2: Stability boundaries at different mass fluxes. $P_i = 700$ [kPa]; $K_i \approx 24$ [-]; and $K_e \approx 5,6$ [-].

A fairly different way to appreciate the implication of the earlier result is shown in Figure 5.3. As expected, by increasing the mass flux the required heat flux for instability inception is increased; and when the inlet subcooling increases the limiting heat flux also increases. Moreover, for all the cases, the increase in the limiting heat flux has shown to be proportional to the increase in the mass flux, meaning that the distance between these curves remains rather constant (approximately 11 [kW/m²] between them). Furthermore, both curves show pretty much the same relative separation from its particular saturated vapor line, showed in the Figure 5.3 by

the dashed lines. These results confirm that the behavior of the necessary heat flux to generate the Density Wave Oscillations is rather similar regardless of mass flux, which is consistent with the results reported by Saha et al. [1976] for a vertical single tube and Colombo et al. [2011] for helical parallel tubes.

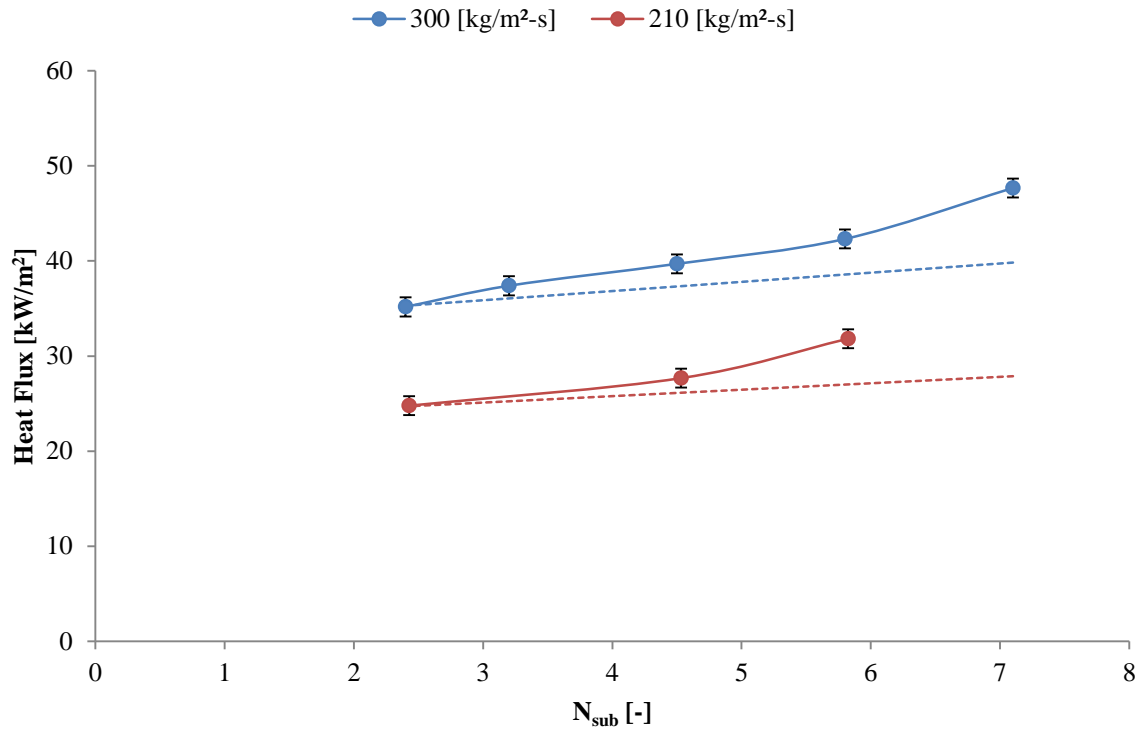


Figure 5.3: Limiting heat flux as function of inlet subcooling for different mass fluxes.

$$P_i = 700 \text{ [kPa]}; K_i \approx 24 \text{ [-]}; \text{ and } K_e \approx 5,6 \text{ [-]}.$$

Beside the previous result, Figure 5.2 also shows that the stable region, which is the region on the left hand side of the stability boundary, increase monotonously as the inlet subcooling is increased. According to the literature (see Table 3.1) this result is in concordance to the stability behavior at “high” subcooling; whereas at “low” subcooling is expected that the stable region decrease by increasing the inlet subcooling. However, in the literature is not well defined what “high” or “low” subcooling is; but considering that the simplified stability criterion of Ishii (see Equation 3.15) is claimed to be valid for Subcooling numbers larger than the number π ($\pi \approx 3,14159$) and has shown to fit well experimental data at high subcooling [Saha et al., 1976], in the present work it is assumed that the transition from “high” to “low” subcooling occurs at Subcooling number equal number π ($T_i \approx 278,0 \text{ [K]}$ at 700 [kPa] for R-134a).

In such case, the data for the lowest Subcooling number ($N_{sub} \approx 2,4$) shows a non-conventional behavior for both mass fluxes, and thereby, the characteristic “L shape” in the stability boundaries are not observed. Similar results were found in the experimental investigation done by Colombo et al. [2011], where the deviation was attributed to the helical shape of the tubes. However, in the present research no conclusion is reached, because it has not been possible to decrease further the inlet subcooling due to the emergence of a different thermally induced two-phase flow instability, which will be discussed in section 4.4.

A final observation can be made regarding the location of the stability boundaries shown in Figure 4.2. For the analyzed system, this lines are located beyond the saturated vapor line (except at low subcooling when are on the line). Theoretically, it means that at the exit of the heated section the fluid will be superheated vapor for most of the operating point on the instability threshold line. However, this would be only the case if thermodynamic equilibrium is assumed; but is well-known that the real systems do not reach equilibrium. As a matter of fact, it has been observed that in the Density Wave Oscillations’ region the flow pattern is annular for all the cases in this research; yielding a significant amount of liquid flow in the mainstream as little droplets and slide on the wall.

5.1.2. Constant heat flux

The collected threshold data, including its uncertainty, for two different heat fluxes are presented in the Ishii-Zuber plane shown in Figure 5.4. These curves are overlapped, as in the case for constant mass fluxes shown in Figure 5.2; which validate the discussion given in the previous section about the importance of the input heat to mass flow rate ratio in the inception of the Density Wave Oscillations. Thus, these results are consistent with Belblidia and Bratianu [1979] conclusion, where they indicate that the Density Wave Oscillations’ are independent of the introduced disturbance to the system to generate it.

Moreover, Figure 5.5 shows that the variation in the supplied heat flux induces a proportional variation in the minimum mass flux that the system can handle before entering in the unstable region. Additionally, it can be seen that by increasing the available heat flux the limiting mass flux is increased; and when the inlet subcooling increase the limiting mass flux decrease.

Regarding the shape of the stability boundary for the constant heat flux case, it can be observed in Figure 4.4 that the bend of the classic “L shape” curve starts at the lowest inlet subcooling ($N_{sub} = 2,40$). However, as was explained in the previous section, it has not been possible to

complete the data set at very low subcooling due to the occurrence of a large amplitude non-periodic instability (see Section 5.4).

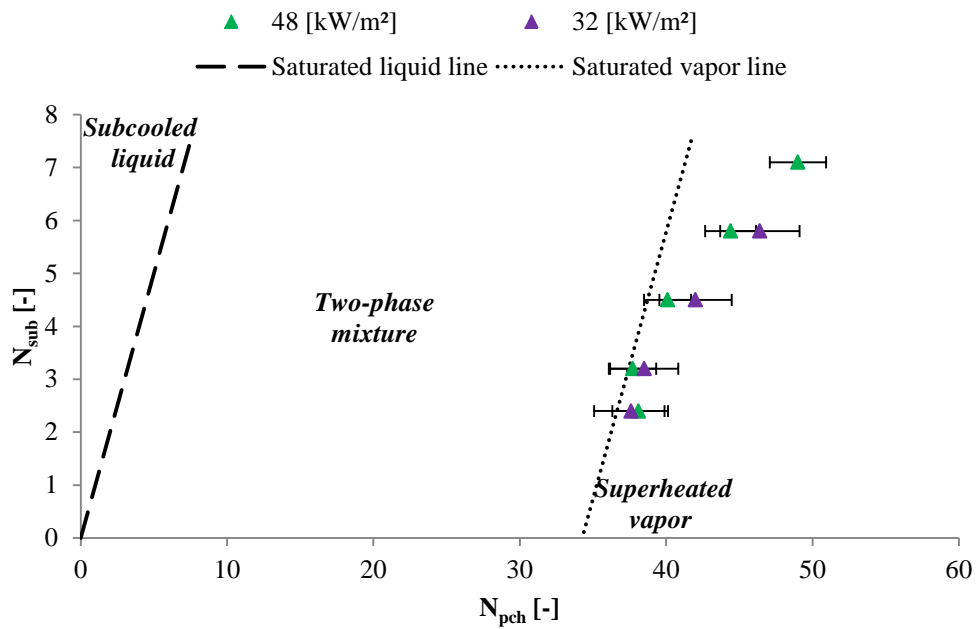


Figure 5.4: Stability boundaries at different heat fluxes. $P_i = 700$ [kPa]; $K_i \approx 24$ [-]; and $K_e \approx 5,6$ [-].

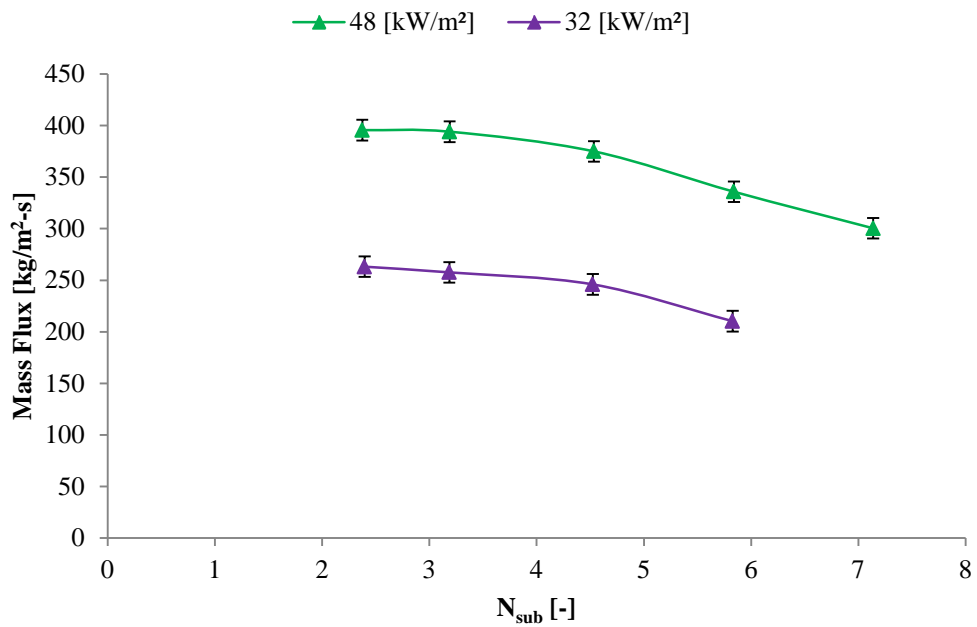


Figure 5.5: Limiting mass flux as function of inlet subcooling for different mass fluxes. $P_i = 700$ [kPa]; $K_i \approx 24$ [-]; and $K_e \approx 5,6$ [-].

Finally, these stability boundaries are found, again, beyond the saturated equilibrium vapor line; but, in these conditions it is still possible to observe some droplets flowing in the mainstream and on the wall at the heated section exit, as an indication that the system is not under thermodynamic equilibrium.

5.1.3. Experimental and Theoretical Threshold Lines

Figure 5.6 shows both experimental and theoretical Density Wave Oscillations' onset for the analyzed system in the present research. For the experimental side, the four stability boundaries introduced in the previous section has been included in the figure; whereas for the theoretical side, the Guido's criterion has been used due to its capability to predict threshold lines in good agreement with other models [Guido et al., 1991].

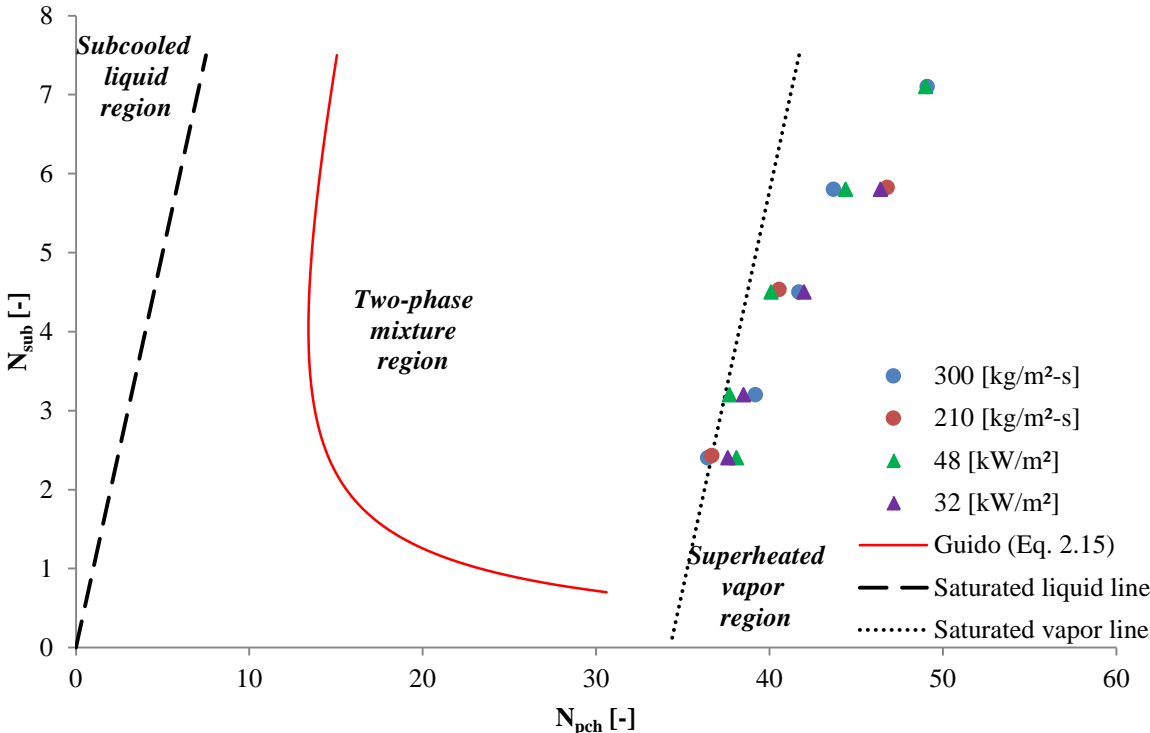


Figure 5.6: Comparison between the stability boundary predicted by Guido's equation and the experimental stability boundary. $P_i = 700$ [kPa]; $K_i \approx 24$ [-]; and $K_e \approx 5,6$ [-].

As it can be easily observed in the figure above, the model predicts an unstable system for a wider range of operating conditions, compared with the actual unstable region experimentally found. This difference between model and experimental results can be attributed to the fact that the Guido's criterion assumes that the pressure drop in the heated section is concentrated at the

inlet and exit flow restrictions, neglecting in such way the effect of the distributed friction. Moreover, most of these simplified models have been probably tuned with data taken from experiments in vertical system, which is in several ways different to the horizontal configuration mainly because in the latter the normal component of the gravitational force promotes stratification in the boiling flow.

Finally, as it can be observed in Figure 5.6, the data taken for different conditions of mass fluxes and heat fluxes seems to be scattered around one single stability boundary. This result is regarded as a final proof about the paramount importance of the heat input to mass flow rate ratio in the determination of the system stability once the geometrical configuration and inlet conditions are established.

5.2. Oscillation Amplitude

According to Belblidia and Bratianu [1979] is usually possible to operate industrial units with some level of fluctuations in the operational parameters. Thereby, the capability for predicting the oscillation amplitude is considered very important. In the following sections a parametrical analysis of the oscillation amplitude will be presented, and thereafter, a new correlation (developed in this work) will be introduced for correlating the experimental data.

However, as the amplitude has shown to be the most sensitive variable within the Density Wave Oscillations' region, it has been necessary to normalize it as follows in order to perform a better analysis.

$$A_{\%} = 100 \frac{A_{p-p}}{2} \frac{1}{\dot{m}} \quad (5.1)$$

where $A_{\%}$ [-] is the amplitude percentage relative to the mean mass flow rate; A_{p-p} [-] is the amplitude peak-to-peak of the mass flow rate oscillation; \dot{m} is the averaged mass flow rate.

5.2.1. Parametrical analysis

In the present research, it has been found that the oscillation amplitude always increases by increasing the heat flux, regardless of inlet subcooling and mass flux, as it is shown in Figure 5.7. It is well-known that the Density Wave Oscillations are caused by multiple regenerative feedbacks between mass flux, void fraction and pressure drop (see Chapter 2). Thus, when the heat flux is increased more energy is introduced to the system; and thereby, the strength of the

regenerative feedbacks increase, which lead to an increase in the oscillation amplitude. This finding is in good agreement with the experimental results reported by Yuncu [1990] and Yuncu et al. [1991].

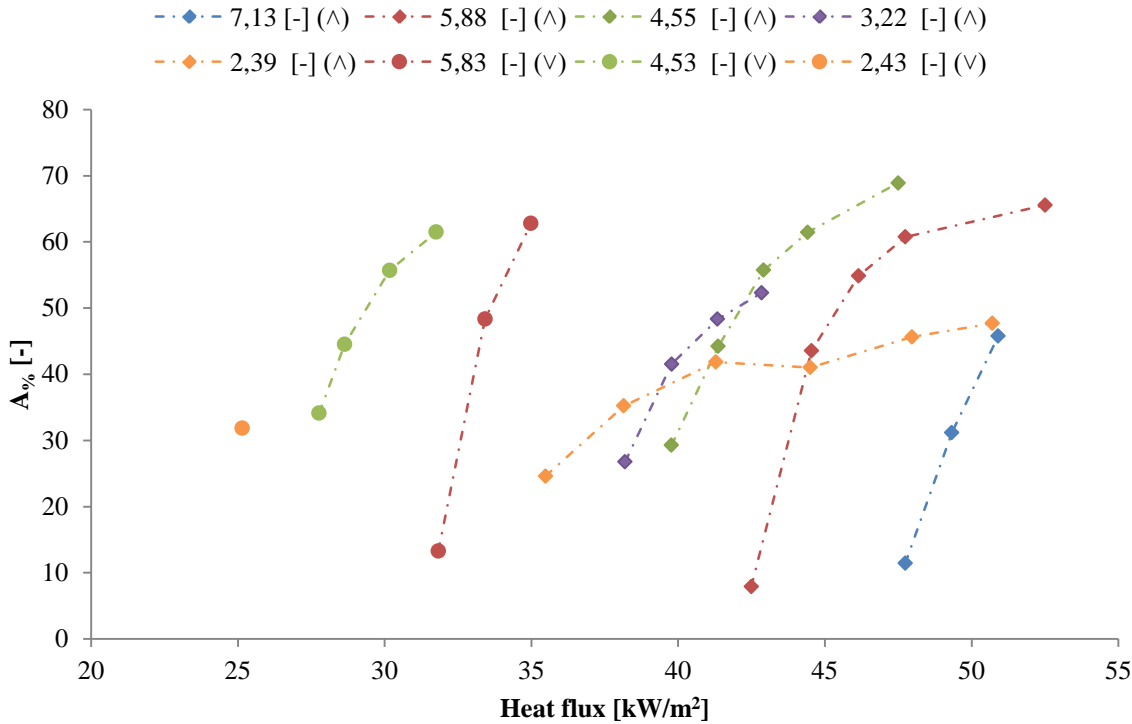


Figure 5.7: Amplitude variation with the heat flux in the Density Wave Oscillations' region at different inlet subcoolings. (Λ) stands for data taken at $m'' = 300$ [kg/m²-s] and (V) stands for data taken at $m'' = 210$ [kg/m²-s]. $P_i = 700$ [kPa]; $K_i \approx 24$ [-]; and $K_e \approx 5,6$ [-].

Furthermore, it can be observed that the amplitude increases very rapidly near to the limiting heat flux, which is the lowest point in each curve, and more slowly as the heat flux increases further. Moreover, it seems like all the curves are increasing towards asymptote, which vary as a function of inlet subcooling and mass flux. According to Lahey and Podowski [1989] the mechanism of Density Wave Oscillation is based on the difference in the propagation velocity for the single-phase region and the two-phase mixture region. Thus, when the heat flux increases the length of the single-phase region (λ) is reduced, as it can be seen in Figure 4.8, due to the increase of energy intake of the system. The effects of the reduction of the single-phase region and the increase in the energy intake of the system are competing at all time. The former induces a damping effect due to the reduction of the single-phase due to vaporization, and this reduces the difference in the propagation velocity, which is a driving force; whereas the latter yield an

increase in the feedback strength, as it was explained earlier. In this way, the amplitude size has a physical limitation imposed by its own formation mechanism because the combined effects of these phenomena lead to a gradual stagnation of the oscillation amplitude.

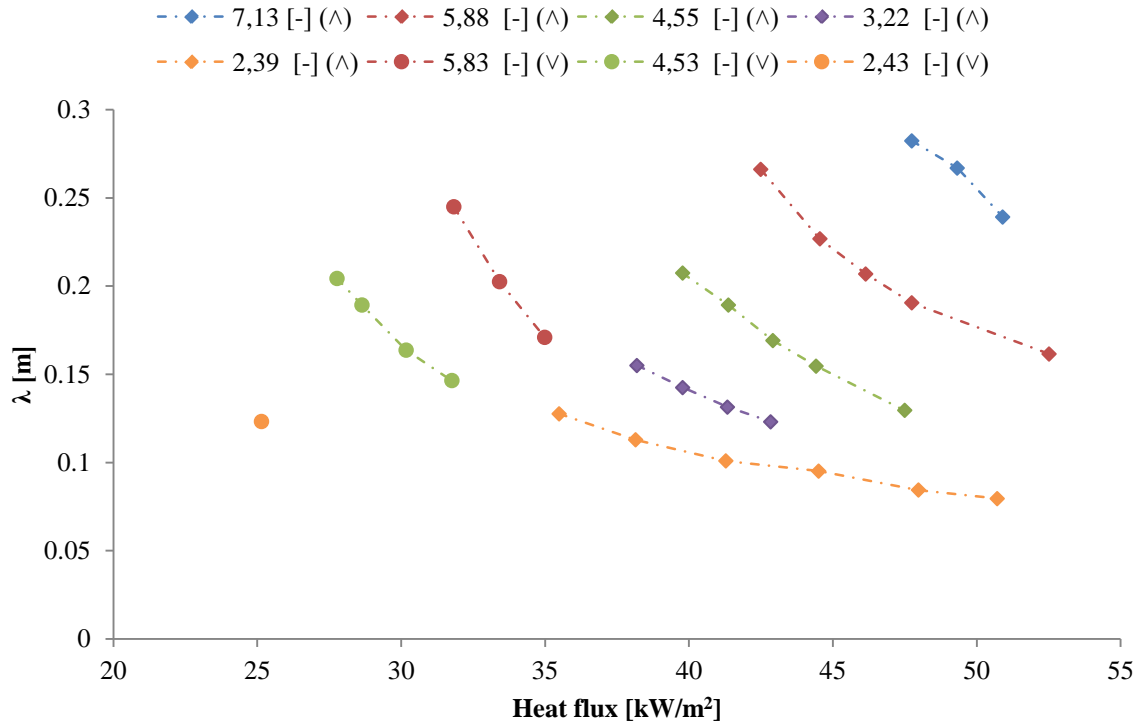


Figure 5.8: Length of the single-phase region as a function of heat flux for different inlet subcoolings. (Λ) stands for data taken at $m'' = 300$ [kg/m²-s] and (V) stands for data taken at $m'' = 210$ [kg/m²-s]. $P_i = 700$ [kPa]; $K_i \approx 24$ [-]; and $K_e \approx 5,6$ [-].

As it can be seen in Figure 5.8, the single-phase region is also reduced by decreasing the inlet subcooling, similar to the findings reported by Wang et al. [1994]. This result may give an explanation to the apparent different maximum asymptotes observed in Figure 5.7. Since lower inlet subcooling yields lower single-phase region, the damping effect is stronger at low subcoolings, due to the reduction in the propagation velocity difference, which reduces the amplitude size. Thus, the already explained combined effect gives lower asymptotes as the inlet subcooling decreases. This effect of the inlet subcooling in the amplitude has been also observed by Mathisen [1967].

5.2.2. Amplitude Correlation

In order to develop a dimensionless correlation for predicting the oscillation amplitude, the Phase Change number is used as x-axis, since it has shown to be useful in the determination of the instability inception for the range of mass flux, heat flux and inlet subcooling investigated in the present research (see Section 5.1). Moreover, it has been included in the analysis the closest stable operating point to the instability threshold condition, such as the operating point at 2550 [s] shown in Figure 5.1; and this is regarded as a point with no amplitude or reference point. Finally, the data has been normalized in the x-axis in such way that the all curves start at the origin, as it can be seen in Figure 5.9 for the data taken at $m'' = 300$ [kg/m²-s].

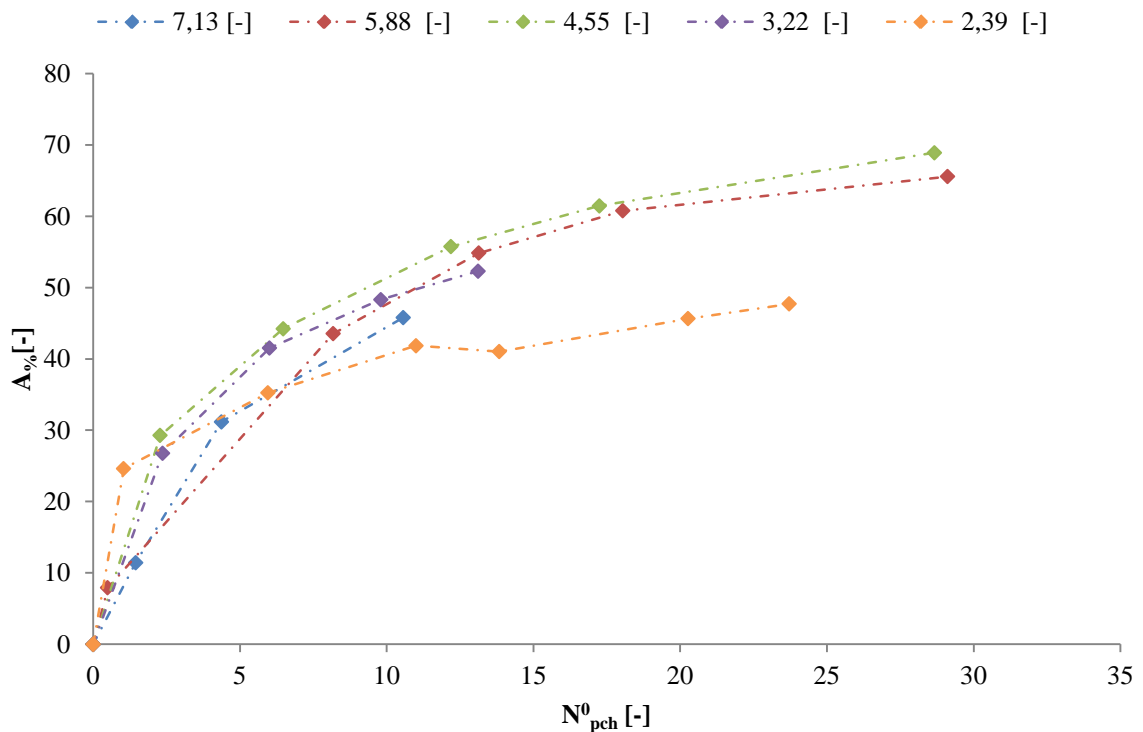


Figure 5.9: Amplitude variation with the normalized Phase Change number in the Density Wave Oscillations' region at different inlet subcoolings. $m'' = 300$ [kg/m²-s]; $P_i = 700$ [kPa]; $K_i \approx 24$ [-]; and $K_e \approx 5,6$ [-].

The above figure shows clearly that all the curves have quite similar behaviors, it increase monotonically until reaches an asymptote, which depend on the inlet subcooling. Moreover, it is remarkable that these curves show a comparable dependency with the void fraction as a function

of flowing quality, as it can be seen in Figure 5.10. This relation was presented in Chapter 2 as follows:

$$\alpha = \frac{1}{1 + \frac{\rho_g}{\rho_l} \left(\frac{1-x}{x} \right) S} \quad (2.24)$$

where α [-] is the void fraction; ρ_g [kg/m^3] and ρ_l [kg/m^3] are the gas and liquid densities respectively; x [-] is the quality; and S [-] is the slip ratio. This last parameter is modeled by Smith's equation [Smith, 1969] for the curves shown in Figure 5.10. This semi-empirical equation is claimed to be valid for all the flow patterns regardless of pressure and mass flux; and it can be written as:

$$S = e + (1 + e) \left[\frac{\left(\frac{\rho_l}{\rho_g} \right) + \left(\frac{1+x}{x} \right)}{1 + e \left(\frac{1+x}{x} \right)} \right]^{\frac{1}{2}} \quad (5.2)$$

where e [-] is the entrained liquid fraction. It should be notice that, the influence of this parameter in the curves shown in Figure 5.10 is similar to the effect of the inlet subcooling in the curves shown in Figure 5.9; that is, both change the growth rate of the curves.

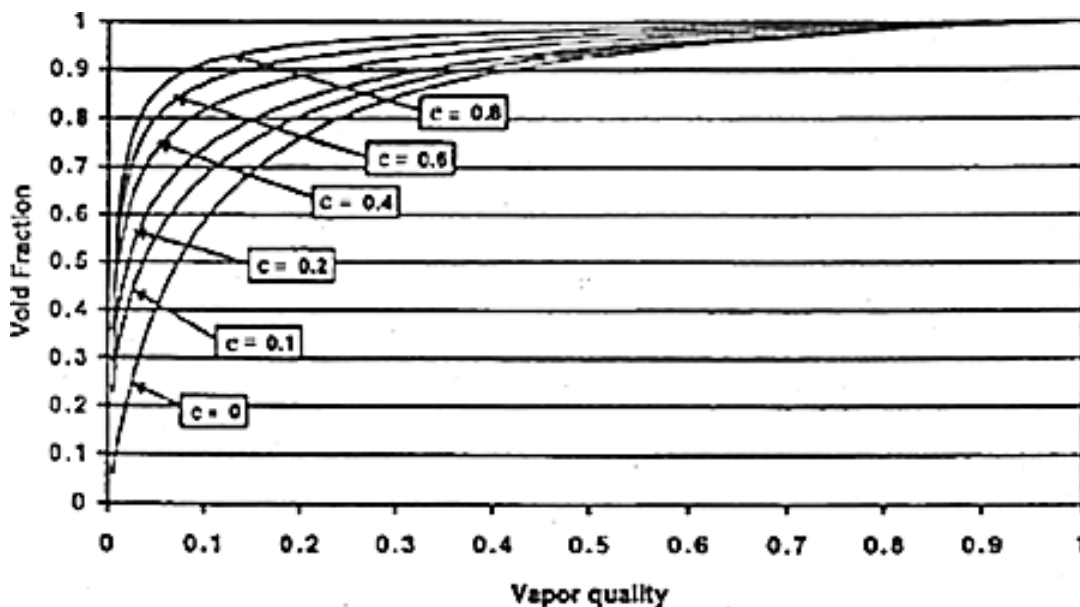


Figure 5.10: Void fraction as a function of flowing quality using the Smith's equation as slip ratio

Based on these similarities, it is proposed, as part of this research, a new correlation to fit the amplitude data. This correlation is pretty similar to the Equation 2.24 for predicting the shape of the curves and includes an empirical parameter in order to take into account the variation of the maximum asymptote with inlet subcooling. Thus, the suggested correlation is presented as follows:

$$A_{\%} = \frac{\Lambda}{1 + \frac{N_{sub}}{N_{pch}^*} \left(\frac{2N_{pch}^* - N_{pch}}{N_{pch} - N_{pch}^*} \right)^{\frac{9}{10}}} \quad (5.3)$$

where Λ [-] is an empirical parameter, which represent the amplitude percentage relative to the mean mass flow rate at a value equal to twice of the critical Phase Change number; and N_{pch}^* [-] is the critical Phase Change number, which is defined as the value when the unstable behavior starts in the system. The above correlation has shown to be valid from the critical Phase Change number on. Moreover, the empirical parameter (Λ) contains information about the asymptotic point at each inlet subcooling; and the Subcooling number to the critical Phase Change number ratio (N_{sub}/N_{pch}^*) [-] contains information about the growth rate at each inlet subcooling. Finally, the suggested correlation show to fit properly all the experimental data collected in the present research, as it can be seen in Figures 5.11 and 5.12.

The experimental data shows that near to the instability inception point the amplitude increases more rapidly at low inlet subcoolings. This feature is well-predicted by correlation, showing that if the inlet subcooling decreases the correlation curve becomes steeper. Additionally, the correlation is capable to predict the data bend in a satisfactory manner regardless of inlet subcooling and mass flux. The broad applicability and predictability of this correlation lies on the fact that it is a function of suitable dimensionless parameters, which are able to describe the system behavior in an appropriate mode. In this sense, it is believed that the suggested correlation is valid at any operational condition within the Density Wave Oscillations' region, since the Phase Change number and the Subcooling number gather most of the relevant information in a boiling flow system.

Finally, the most promising feature of the present correlation is related to the fact that it is possible to estimate the maximum oscillation value for a given inlet subcooling regardless of mass flux, as it can be seen in Figures 5.13 and 5.14.

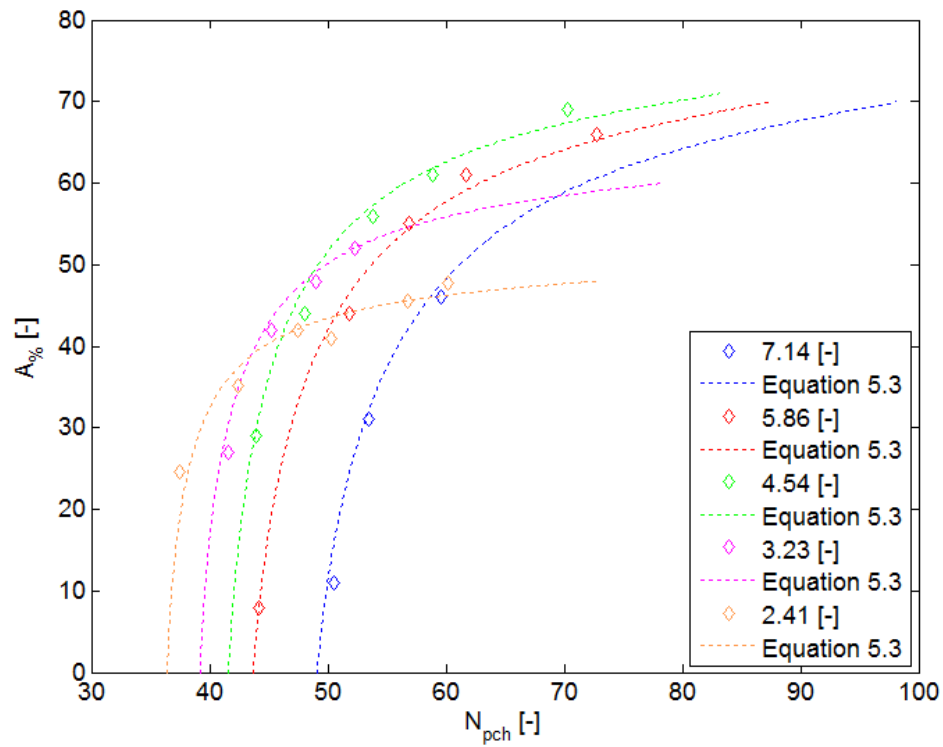


Figure 5.11: Amplitude variation with the Phase Change number at different inlet subcoolings and correlation curves. $m'' = 300$ [kg/m²-s]; $P_i = 700$ [kPa]; $K_i \approx 24$ [-]; and $K_e \approx 5,6$ [-].

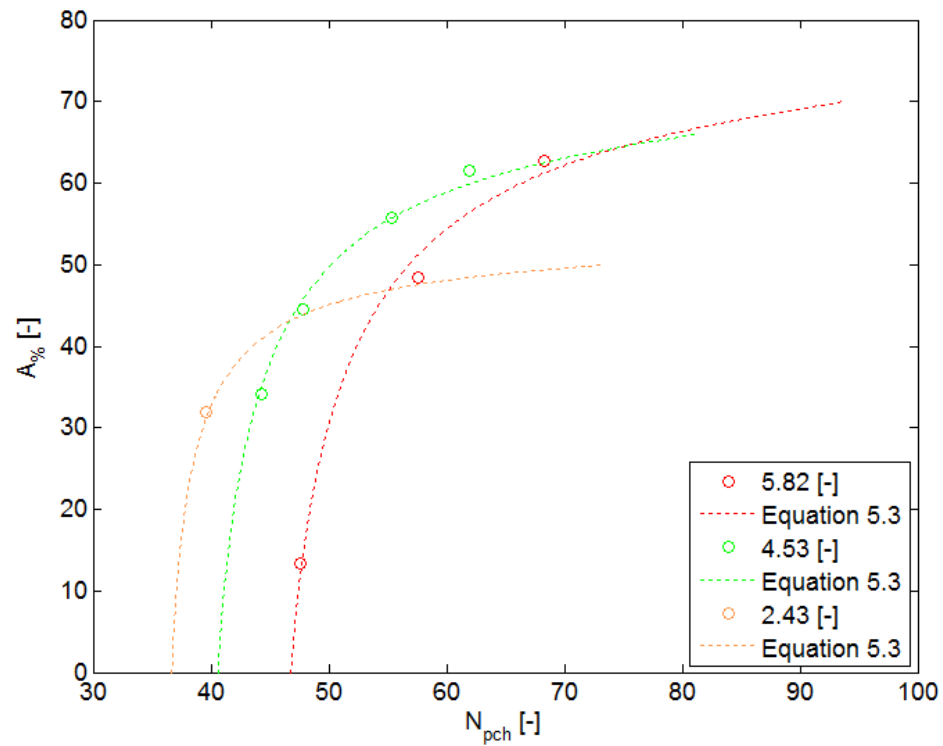


Figure 5.12: Amplitude variation with the Phase Change number at different inlet subcoolings and correlation curves. $m'' = 210$ [kg/m²-s]; $P_i = 700$ [kPa]; $K_i \approx 24$ [-]; and $K_e \approx 5,6$ [-].

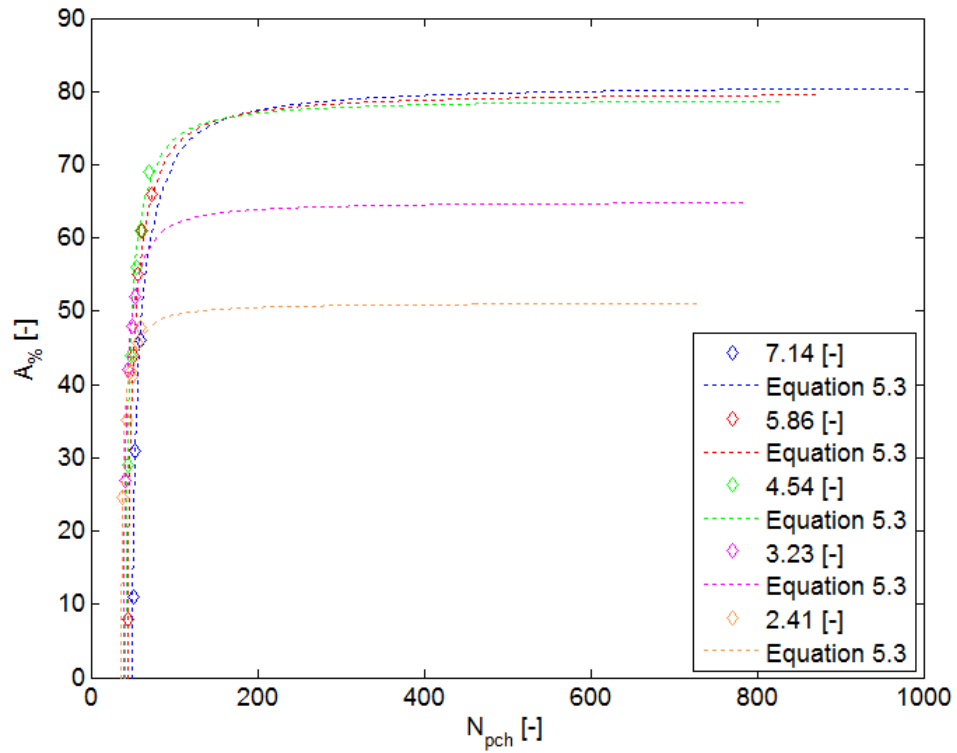


Figure 5.13: Prediction of the maximum amplitude at different inlet subcoolings.
 $m'' = 300$ [kg/m²-s]; $P_i = 700$ [kPa]; $K_i \approx 24$ [-]; and $K_e \approx 5,6$ [-].

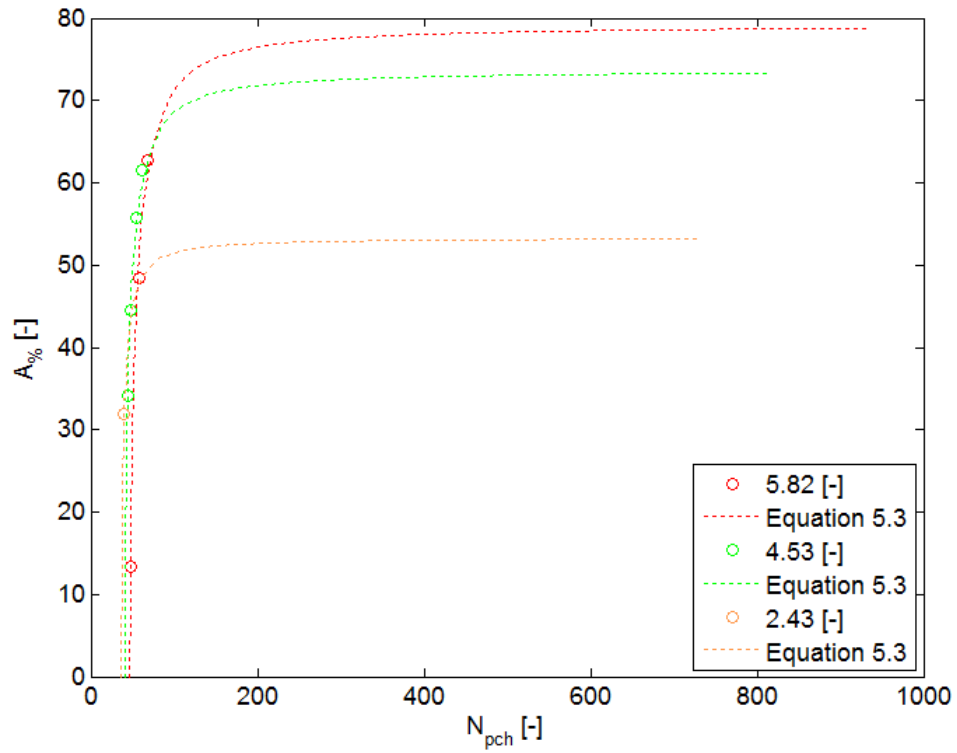


Figure 5.14: Prediction of the maximum amplitude at different inlet subcoolings.
 $m'' = 210$ [kg/m²-s]; $P_i = 700$ [kPa]; $K_i \approx 24$ [-]; and $K_e \approx 5,6$ [-].

As it was discussed earlier in this section, by increasing the inlet subcooling the maximum oscillation should increase; and as it is shown in Figures 5.13 and 5.14 the correlation follows this expected trend regardless of mass flux. This capability of Equation 5.3 for predicting the maximum oscillations values has significant implications on the design and operational control in units susceptible to the occurrence of Density Wave Oscillations. However, it should be mentioned that, it was not possible to verify in the experimental facility the prediction provided by this correlation, due to operational restrictions related the thermal limitation in the rig.

5.3. Oscillation Period

Conversely to what is shown for the oscillation amplitude, the period oscillation decrease by increasing the heat flux regardless of inlet subcooling and mass flux, as can be seen in Figure 5.15. As it was discussed in this chapter, by increasing the heat flux the length of the single-phase region is decreased (see Figure 5.8); and thus, the averaged residence time of a fluid particle will decrease. A shorter residence time means a greater propagation velocity in the system; and thereby, the lag in the feedback response is decreased yielding a reduction in the oscillation period. This result is in accordance with the experimental findings of some researchers, such as Yuncu et al. [1991], Wang et al. [1994] and Ding et al. [1995]. Furthermore, this figure also shows that the oscillation period decreases by decreasing the inlet subcooling, which is due to the reduction of the single-phase region as well. This observation can be more easily seen in Figure 4.16, showing that the effect is observed regardless of heat flux and mass flux.

Moreover, in Figure 4.15 it can be observed that by decreasing the mass flux the period is increased. This result is totally expected since a reduction in the mass flux increase the averaged particle residence time due to the reduction in the propagation velocity. As the propagation velocity decreases the lag in the system feedback will increase, which lead to increment the oscillation period.

In addition to the previous observations, a closer look at Figure 4.15 shows that all the curves seem to be decreasing towards minimum asymptotes, which are particular for each inlet subcooling for a given mass flux. This result is directly derived to the maximum amplitudes discussed in the previous section, since it has been experimentally observed that the period decrease when the amplitude is increased.

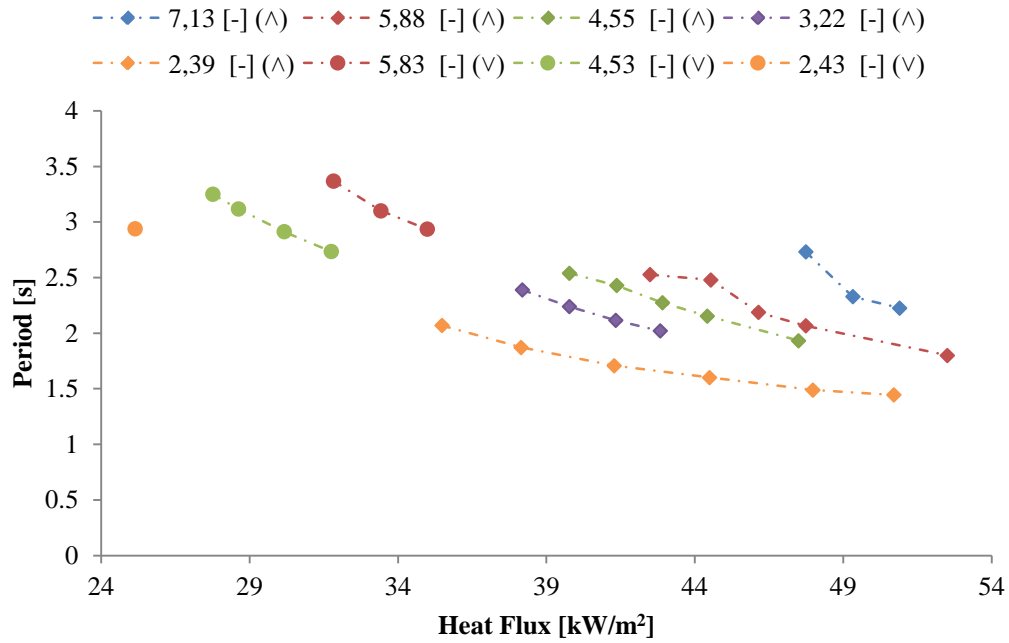


Figure 5.15: Period variation with the heat flux in the Density Wave Oscillations' region at different inlet subcoolings. (\wedge) stands for data taken at $m'' = 300$ [kg/m²-s] and (\vee) stands for data taken at $m'' = 210$ [kg/m²-s]. $P_i = 700$ [kPa]; $K_i \approx 24$ [-]; and $K_e \approx 5,6$ [-].

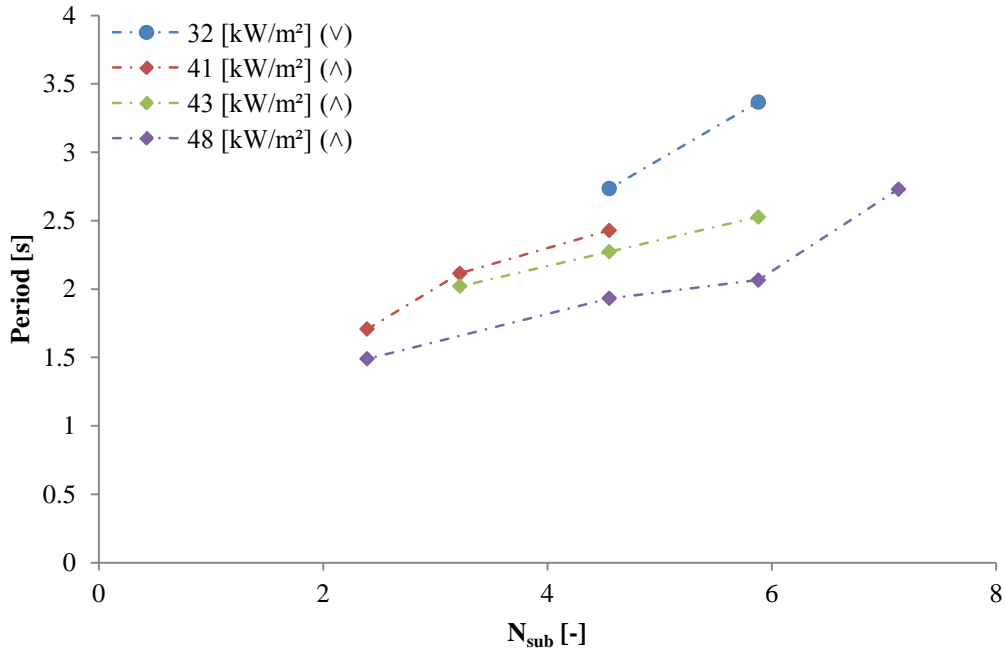


Figure 5.16: Effect of the inlet subcooling on the oscillation period at different heat fluxes and mass fluxes. (\wedge) stands for data taken at $m'' = 300$ [kg/m²-s] and (\vee) stands for data taken at $m'' = 210$ [kg/m²-s]. $P_{inlet} = 700$ [kPa]; $K_i \approx 24$ [-]; and $K_e \approx 5,6$ [-].

Regarding the shape of the curves shown in Figure 5.15, it can be observed some similarities with the curves shown in Figure 5.8. This correspondence indicates a sort of relationship between the oscillation period and the length of the single-phase region. Figure 5.17 shows that the oscillation period has a linear relation with the single-phase residence time regardless of mass flux and inlet subcooling. This single-phase residence time is related to the length of the single-phase region by the following expression:

$$\tau_{sp} = \frac{\lambda}{u_i} = \lambda \frac{\rho_i}{m''} \quad (5.4)$$

where τ_{sp} [s] is the single-phase residence time; u_i [m/s] is the velocity at the inlet of the heated section; and ρ_i [kg/m³] is the fluid density at the inlet of the heated section. These results are in good agreement with the experimental findings reported by Aritomi et al. [1979]; and its importance lies on the relation shown between the single-phase region and both oscillation amplitude and period.

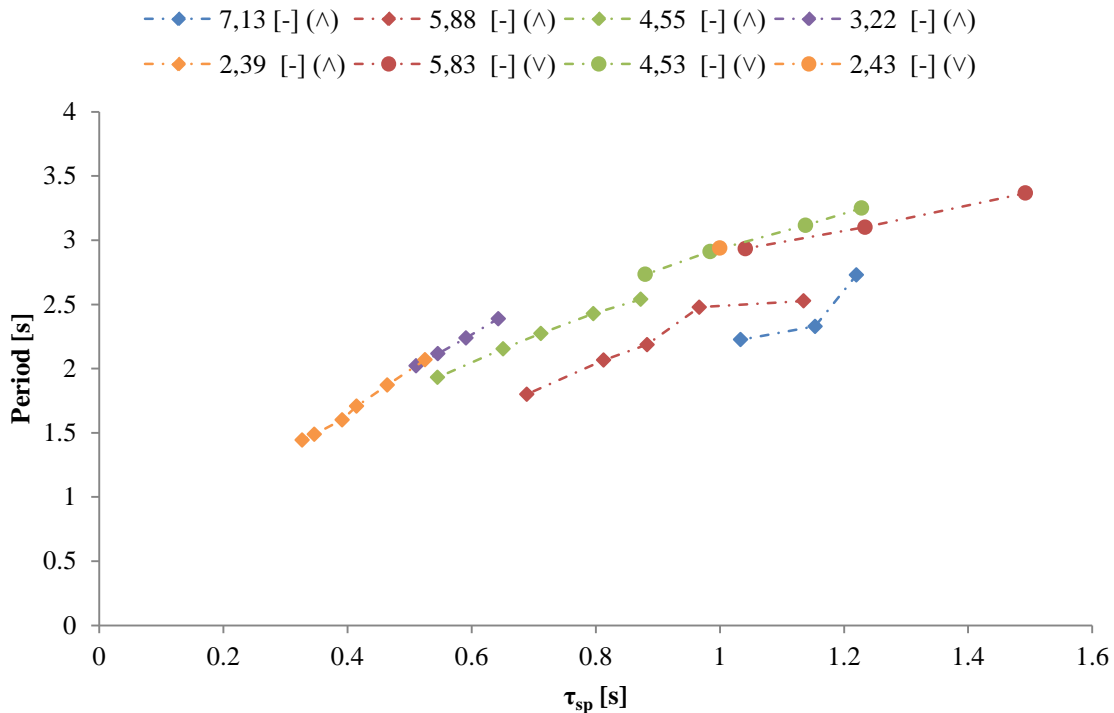


Figure 5.17: Oscillation period as a function of the single-phase residence time for different inlet subcoolings. (\wedge) stands for data taken at $m'' = 300$ [kg/m²-s] and (\vee) stands for data taken at $m'' = 210$ [kg/m²-s]. $P_i = 700$ [kPa]; $K_i \approx 24$ [-]; and $K_e \approx 5,6$ [-].

5.4. Boundaries of the Experimental Data

The range of inlet subcoolings investigated has been restricted by the facility thermal limitation and the presence of a different kind of thermal induced instability. The former restriction has imposed the upper boundary of the inlet subcooling, since it has avoided the possibility of reaching the instability inception point at inlet temperatures below 273 [K] when the system is operated at inlet pressure of 700 [kPa]. In the other hand, the latter restriction has imposed the lower inlet subcooling boundary, since the unknown instability has been observed only at inlet temperatures above 291 [K] when the system is operated at inlet pressure of 700 [kPa]. In the following sections a brief discussion of these restrictions will be presented and the characteristic traces of the most relevant operational parameter will be introduced for each case.

5.4.1. Upper Boundary

As stated before this boundary is imposed by the thermal limitation of the facility, which is supposed to operate at temperatures below 373 [K] on the tube wall in order to avoid a burn-out. Figure 5.18 shows a characteristic case where the temperature at the outlet of the tube wall is slightly above the allowed temperature in the heated section before observing a well-defined self-sustained periodic oscillation with constant amplitude; and thereby this case cannot be considered as a point belonging to the Density Wave Oscillations' region.

The reason behind this phenomenon can be explained considering the behavior of the limiting heat flux shown in Figure 5.3. As can be seen in that figure, the distance between the limiting heat flux and the saturated vapor line is increased by increasing the inlet subcooling. This yields an increase in outlet wall temperature since at this point most of the fluid has been evaporated.

5.4.2. Lower Boundary

In this case a non-periodic instability arises and it is totally different to the typical Density Wave Oscillations. The characteristic traces of this instability are presented in Figure 5.19, where some differences relative to the typical Density Wave Oscillation behavior (see Figure 4.5) can be appreciated.

The main difference between these instabilities is observed in the mass flux trace, since the two-phase flow instability shown in Figure 5.19 displays non-uniform amplitude and high values of amplitude peak-to-peak, which are classic characteristic of a Geysering type of instability [Yun et al., 2005]. Similar kind of unstable behavior have been experimentally found and analyzed by Masanori et al. [1993], Jiang et al. [1995] and Wang et al. [1996].

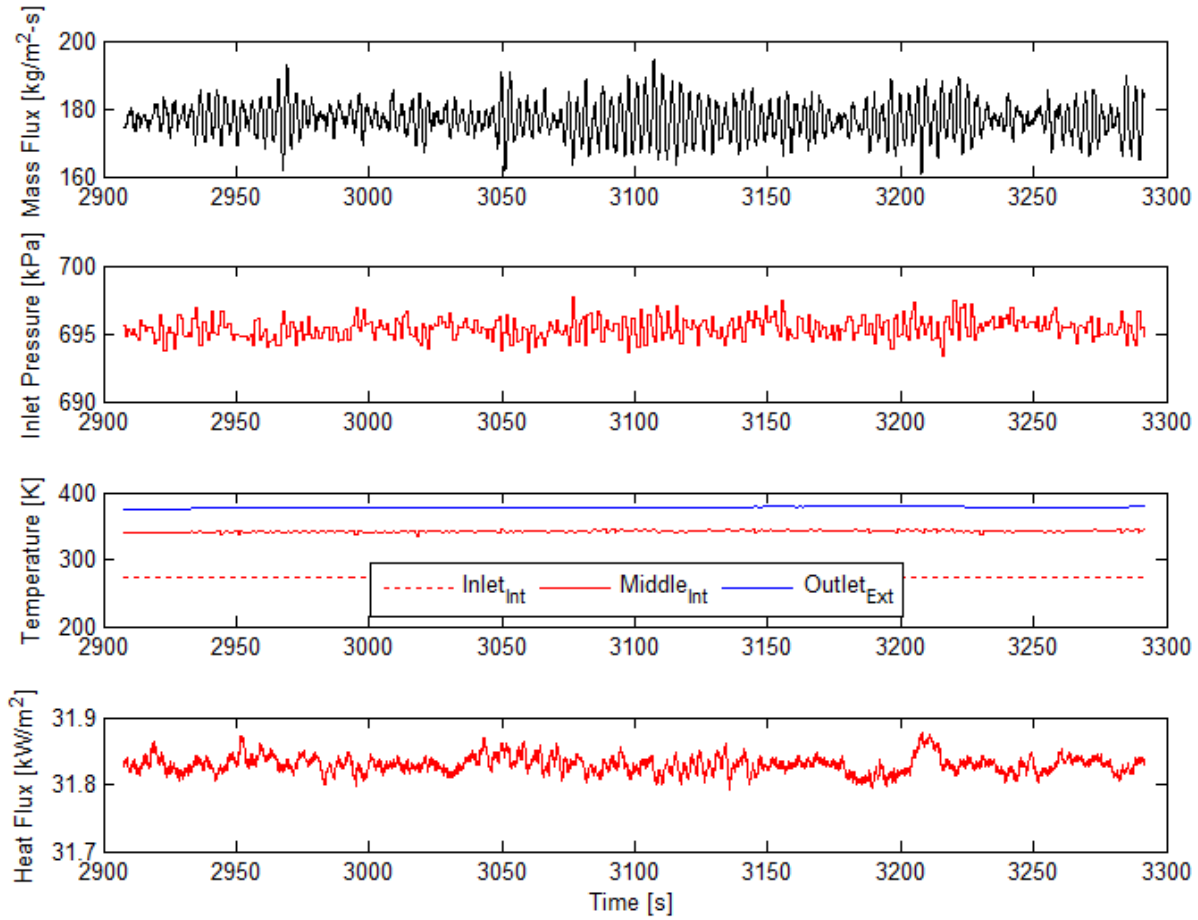


Figure 5.18: Typical traces at high inlet subcooling values when the facility thermal limitation is reached before observing Density Wave Oscillations. $m'' = 175$ [kg/m²-s]; $P_i = 695$ [kPa]; $T_i = 273,8$ [K]; $q'' = 32$ [kW/m²]; $K_i \approx 24$ [-]; $K_e \approx 5,6$ [-]; and $T_o = 378,9$ [K].

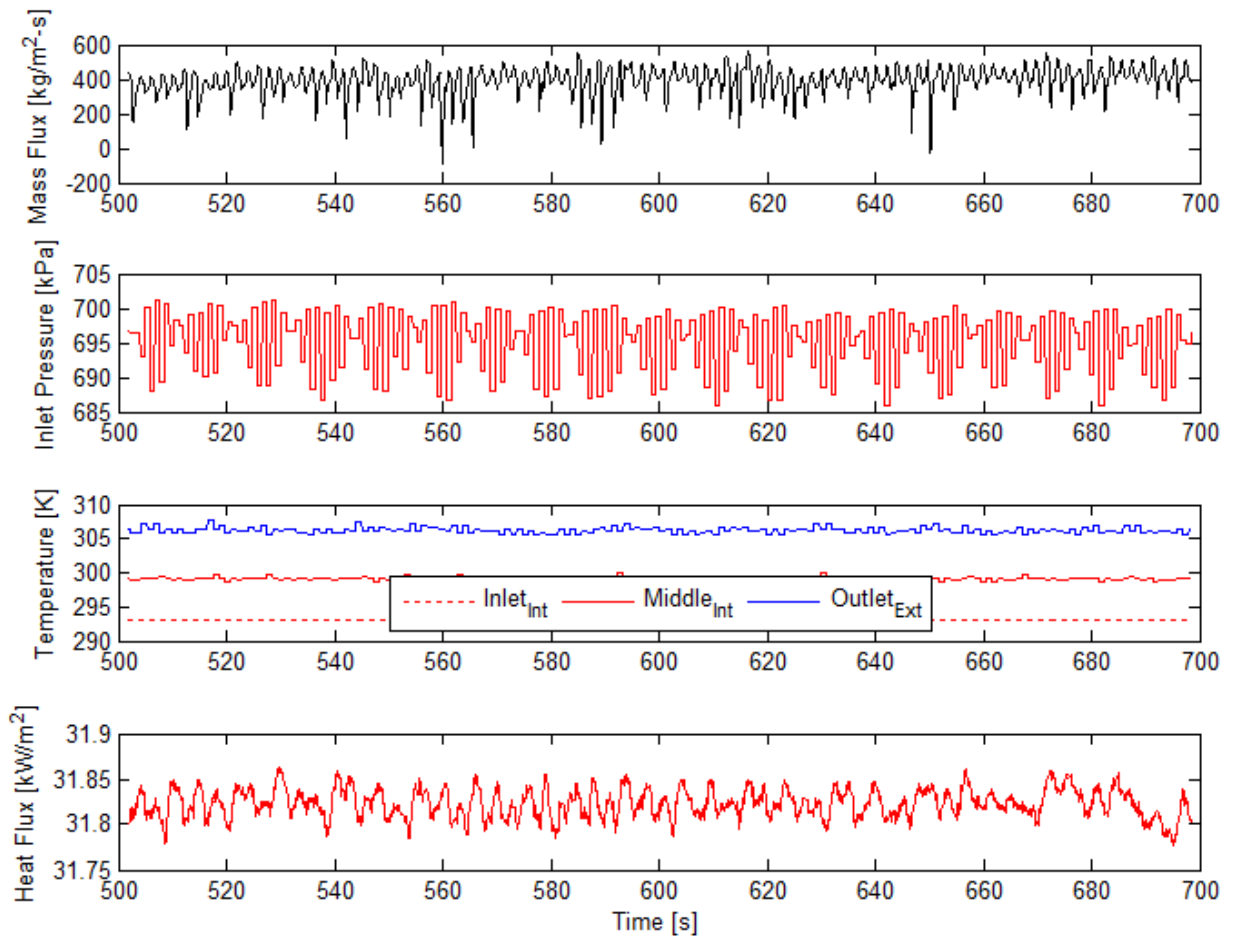


Figure 5.19: Typical traces of instability found at low inlet subcooling. $m'' = 175$ [kg/m²-s];
 $P_i = 695$ [kPa]; $T_i = 293,1$ [K]; $q'' = 32$ [kW/m²]; $K_i \approx 24$ [-]; $K_e \approx 5,6$ [-];

CHAPTER 6

CONCLUSIONS

The influence of the main operational parameters in the occurrence and characteristic of the most frequent two-phase flow instability, namely Density Wave Oscillations, is addressed in the present experimental research for a single horizontal boiling channel. The Ishii-Zuber plane is found to be appropriate to represent the system stability since for given geometrical configuration of the boiling channel and inlet conditions of the working fluid the heat input to the mass flow rate ratio (q/\dot{m}) [J/kg] define the onset of Density Wave Oscillations, regardless whether the system is operating at constant mass flux or at constant heat flux.

In addition, it is found that Guido's criteria predicts an unstable system for a wider range of operating conditions compared with the experimental data; and thereby, cannot be used to estimate the instability threshold in the analyzed system.

For operating conditions in the unstable region, the amplitude monotonically increases by increasing the heat flux until it reaches an asymptote. This asymptote depends on the inlet subcooling and mass flux. Moreover, the period is found to decrease when the amplitude is increased; and, as a consequence, the period decreases monotonically until reaches an asymptote.

The described behavior has significant implications on the system control. The value of maximum amplitude determines the necessary control action if and when the system becomes unstable. In this sense, a new dimensionless correlation based on amplitude ratio, is proposed as a result of the observed trends. It is found to be very useful, not only correlates well the collected data at the onset of Density Wave Oscillation, but also predicts the maximum amplitude for the given sets of operating conditions.

CHAPTER 7

RECOMMENDATIONS FOR FUTURE WORKS

Since in the present research it was not possible to verify experimentally the maximum amplitudes predicted by the new correlation introduced in this work, it is highly recommended to perform an experimental investigation to further analyze the effect of different operational parameter in the maximum amplitude values. Such analysis might help to designers to assess the maximum risk of operating in the Density Wave Oscillations' region.

On the other hand, regarding the occurrence of non-periodic large-amplitude oscillations a low inlet subcooling (see Figure 5.19), it is suggested to perform new experiments in order to fully understand the mechanism of formations and characteristics of this unknown thermal-hydraulic instability.

REFERENCES

- Aldridge, C. J. & Fowler, A. C., Stability and instability in evaporating two-phase flows, *Surveys on Mathematics for Industry*, **1996**, 6, 75-107.
- Aritomi, M.; Aoki, S. & Inoue, A., Instabilities in parallel channel of forced-convection boiling upflow system, *Journal of Nuclear Science and Technology*, **1979**, 14, 88–96.
- Belblidia, L. & Bratianu, C., Density-wave oscillations, *Annals of Nuclear Energy*, **1979**, 6, 425-444.
- Boure, J.; Bergles, A. E. & Tong, L. S., Review of two-phase flow instability, *Nuclear Engineering and Design*, **1973**, 25, 165-192.
- Collins, D. B. & Gacesa, M., Hydrodynamic instability in a full-scale simulated reactor channel, *Proceedings of the Institution of Mechanical Engineers*, **1969**, 184, 115–126.
- Ding, Y.; Kakac, S. & Chen, X. J., Dynamic instabilities of boiling two-phase flow in a single, horizontal channel, *Experimental Thermal and Fluid Science*, **1995**, 11, 327–342.
- Guido, G.; Converti, J. & Clause, A., Density-wave oscillations in parallel channels-an analytical approach, *Nuclear Engineering and Design*, **1991**, 125, 121-136.
- Ishii, M. & Zuber, N., Thermally induced flow instabilities in two-phase mixtures, *Fourth International Heat Transfer Conference*, **1970**, B5, Paper No. 11.
- Kakac, S. & Bon, B., A review of two-phase flow dynamic instabilities in tube boiling systems, *International Journal of Heat and Mass Transfer*, **2008**, 51, 399–433.
- Komakli, O.; Karsli, S. & Yilmaz, M., Experimental investigation of two-phase flow instabilities in a horizontal in tube boiling system, *Energy Conversion and Management*, **2002**, 43, 249–268.
- Maulbetsch, J. S. & Griffith, P., A study of system-induced instabilities in forced-convection flows with subcooled boiling, *Massachusetts Institute of Technology*, **1965**.
- Rizwan-Uddin & Dorning, J., Some nonlinear dynamics of a heated channel, *Nuclear Engineering and Design*, **1986**, 93, 1-14.

Ruspini, L. C., Experimental and modeling study of two phase flow instabilities in single channel, *NTNU*, **2012**.

Saha, P.; M. Ishii & Zuber, N., Experimental investigation of the thermally induced flow oscillations in two-phase systems, *Journal of Heat Transfer*, **1976**, 4, 616–622.

Smith, S. L., Void fractions in two-phase flow: a correlation based upon an equal velocity head model, *Proceedings of the Institution of Mechanical Engineers*, **1969**, 184, 647-664.

Yadigaroglu, G. & Bergles, A. E., An experimental and theoretical study of density-wave oscillations in two-phase flow, *Massachusetts Institute of Technology*, **1969**.

Yuncu, H.; Yildirim, O. T. & Kakac, S., Two-phase flow instabilities in a horizontal single boiling channel, *Applied Scientific Research*, **1991**, 48, 83-104.